J. Fluid Mech. (2000), *vol.* 404, *pp.* 345–378. Printed in the United Kingdom

Control of global instability in a non-parallel near wake

By TZONG-SHYNG LEU AND CHIH-MING HO

Department of Mechanical, Aerospace and Nuclear Engineering, University of California, Los Angeles, Los Angeles, CA 90095-1597, USA

(Received 12 November 1996 and in revised form 28 September 1999)

The effect of base suction on a plane wake was found to produce significant changes in wake dynamics. The wake is produced by merging two boundary layers from the trailing edge of a splitter plate in a two-stream water tunnel. A threshold suction speed exists which is approximately equal to half of the free-stream velocity. If the suction speed is below the threshold, the wake flow is unstable. If the suction speed is above the threshold, the wake becomes stable and no vortex shedding is observed. In the present experiment, the suction technique can stabilize a wake at a maximum tested Reynolds number of 2000.

The suction significantly reduces the length of the absolutely unstable region in the immediate vicinity of the trailing edge of the splitter plate and produces a non-parallel flow pattern, resulting in the breakdown of global instability. The global growth rate changes from positive (unstable flow) to negative (stable flow) at the suction speed equalling 0.46 of the free-stream velocity. The threshold suction speed can be accurately predicted by the global linear theory of Monkewitz *et al.* (1993) with a non-parallel flow correction.

1. Introduction

The vortex shedding that appears downstream from bluff bodies above a critical Reynolds number has been studied since the turn of this century. Vortex shedding induces drag, generates noise and causes structure vibration. During the past few decades, several techniques have been developed to control it. Roshko (1955) investigated wake control methods to reduce the drag on the flow past a circular cylinder. A thin partition placed along the centreline of the wake, downstream of the cylinder, extending four or five diameters, was found to prevent Kármán-type vortex shedding and reduce the drag coefficient from 1.1 to 0.7. Similarly, Wood (1964, 1967) reduced the strength of individual vortices by blowing at the trailing edge.

After 1985, the concepts of absolute and convective instabilities (Huerre & Monkewitz 1985, 1990) have provided new physical insights into wake control. The difference between absolute instability and convective instability is that the impulse response of a fluid system can propagate in both upstream and downstream directions in an absolutely unstable flow, whereas it can only propagate in the downstream direction in a convectively unstable flow region. Therefore, a flow system that contains a sufficiently large region of absolute instability will respond to external forcing by developing time-amplifying global oscillations, a response that is fundamentally different from that of a system that is convectively unstable everywhere. In free shear layer flow, the

absolute instability analysis was first applied in the mixing layer by Huerre & Monkewitz (1985). The mixing layer becomes absolutely unstable when two free streams are in opposite directions and the back flow (negative) velocity is greater than 0.135 of the forward flow (positive) velocity. In jet flow, Strykowski & Niccum (1991) observed the onset of absolutely unstable flow oscillations in an axisymmetric counter-flowing jet when the back flow velocity is greater than 0.138 of the jet velocity. In wake flow, both types of instability exist. The near wake is governed by absolute instability. The wake then changes to convective instability at a short distance from the solid boundary due to the rapid filling of the velocity deficit. In the absolutely unstable region, wake flow acts as a resonator where all unstable disturbances are self-excited or time-amplified. In the convectively unstable region, wake flow is similar to a spatial amplifier in that all unstable frequencies (for small-amplitude perturbations) will grow exponentially along the downstream direction. Therefore, the disturbances will first resonate in the absolutely unstable region and then serve as an initial perturbation in the convectively unstable region.

Numerical and experimental evidence indicates that the wake instabilities are strongly influenced by an absolutely unstable region in the near wake. This fact suggests the possibility of controlling global flow characteristics through modification of the streamwise velocity profiles at the origin of wake flow. Some methods for controlling Kármán vortex shedding in the near wake have been proposed, and are briefly reviewed in the following. Wood (1964, 1967) demonstrated the effects of reducing the strength of individual vortices by blowing at the trailing edge. Bearman (1967) also demonstrated that sufficient base bleed leads to a reduction of base drag. Hanneman & Oertel (1989) successfully suppressed vortex shedding from bluff bodies by bleeding fluid from the blunt base in their numerical simulation. Strykowski & Sreenivasan (1990) placed a small control cylinder with a diameter of typically $\frac{1}{8}$ to $\frac{1}{20}$ of the primary cylinder diameter in the near wake of the primary cylinder and suppressed vortex shedding at a Reynolds number of about 80. The most effective location for the suppression of vortex shedding is generally in the shear layers around the mean recirculation region. The effect of the control cylinder is speculated to be the breaking of the mean flow symmetry and the cancellation of the vorticity which are responsible for the reduction of absolute instability. Another well-known method for suppression of vortex shedding from bluff bodies at a low Reynolds number is through heat addition to the near wake. The connection of this effect to local stability properties was investigated by Yu & Monkewitz (1990). The primary purpose of heating was to decrease local absolute growth rates by reducing the fluid density of the near wake. The above mentioned studies have shown that Kármán vortex shedding can be significantly manipulated by a small modification to the near wake. However, most of these control techniques are effective only at a low Reynolds number. In the present study, base suction is used to provide an approach to wake flow control at a Reynolds number of 2000, the wake becoming globally stable (Leu & Ho 1992*a*, *b*, 1993). This experimental finding is consistent with the numerical simulation works of Hammond & Redekopp (1997) where a non-dimensional threshold suction speed of 0.4 is reported at $Re = 120$ (for uniform suction profile).

The paper is based on Leu's PhD thesis (1994). Flow visualization experiments are first used to present the remarkable change in a wake flow with suction control. Then, the threshold suction speed is determined and the stability characteristics of the wake flow are identified by experimental methods. The changes of the near-wake flow field from subcritical to supercritical suction are examined. Finally, the prediction of the threshold suction speed, based on the global linear theory of Monkewitz, Huerre &

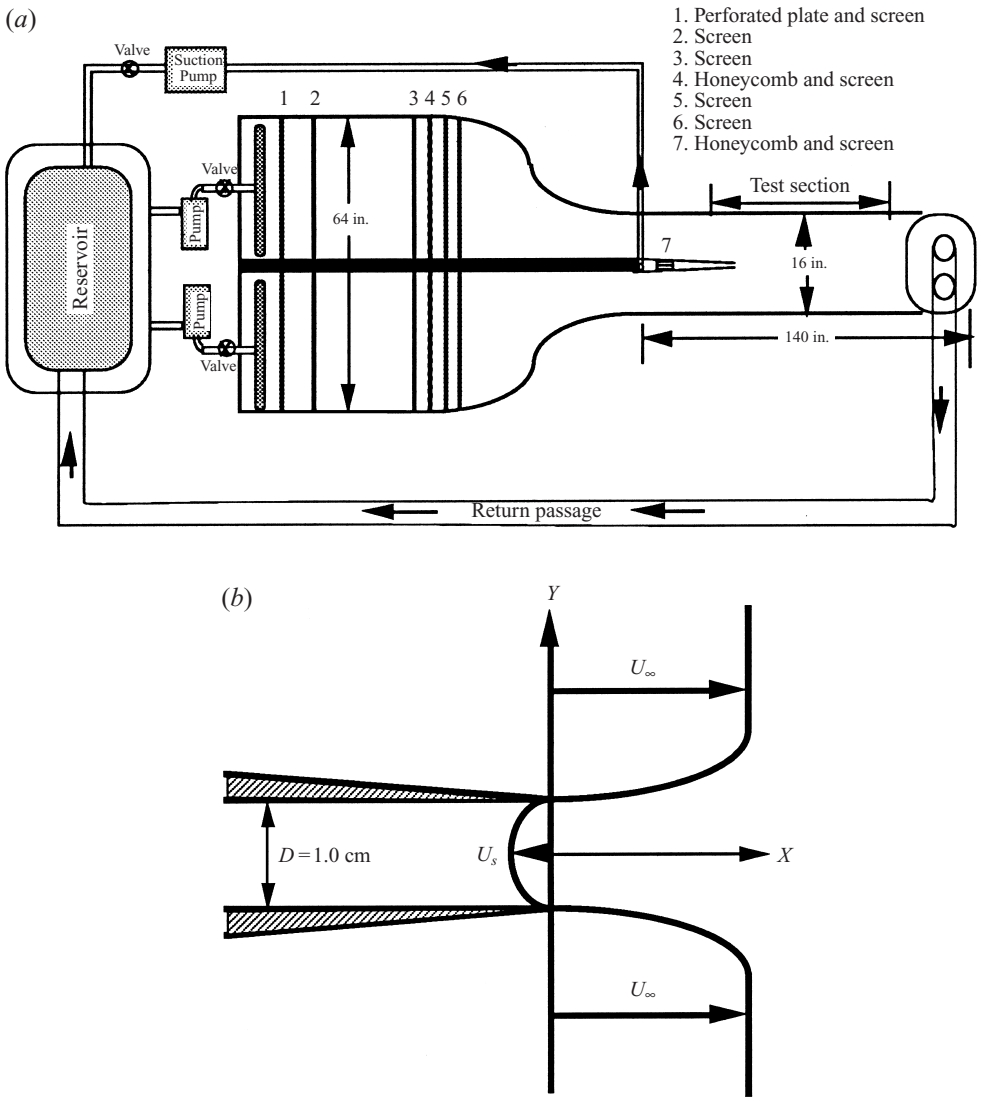

FIGURE 1. (*a*) Schematic of the water channel (not drawn to scale). (*b*) Trailing edge configuration and coordinate system.

Chomaz (1993), and the description of wake flow dynamics by the Stuart–Landau equation are presented.

2. Experimental facilities and instrumentation

The experiments were performed in an open surface water channel. Figure 1(*a*) shows a sketch (not to scale) of the water channel. The channel was designed for studies of the wake/mixing layer. The stagnation chamber is separated into two compartments by a vertical splitter plate. Flow in each compartment is supplied by a pump. Each pump is controlled by a valve. The velocity ratio between the two free streams can be easily adjusted by these two valves. The water channel includes three parts: a stagnation chamber, a splitter plate and a test section. Water is pumped

from the reservoir into the stagnation chambers. A perforated plate, honeycomb and six layers of screens are used to improve the flow uniformity and to reduce the turbulence level. The splitter plate is placed vertically to avoid the troublesome problem of removing air bubbles from the screens. The test section is equipped with a glass window on top to eliminate the free-surface wave. The width and height of the test section of the water channel are 40.0 and 20.0 cm respectively. The maximum free-stream velocity U_∞ is 20 cm s^{-1}. The typical turbulence level in the test section is about 0.6% of the time-averaged velocity. At the end of the water channel, two 4 in. diameter PVC pipes serve as return passages to the upstream reservoir. The trailing edge of the splitter plate (figure 1*b*) is a suction slot with width $D = 1.0$ cm. Throughout the paper the Reynolds number is based on the free-stream velocity U_∞, and the width of the suction slot D. The spanwise dimension of the suction slot is $20D$ and the Z-coordinate from the bottom wall to the top glass window in the test section is $Z/D = 0$ to 20. Inside the hollow splitter plate region, a perforated tube is connected to a third pump. The third pump provides suction at the trailing edge of the splitter plate. Two fine mesh screens and a plastic honeycomb section made of stacks of straws are placed between the perforated tube and suction slot to reduce the turbulence level and the non-uniformity of suction in the spanwise direction. The configurations of the trailing edge and coordinate system are shown in figure 1(*b*). The suction speed U_s (figure 1*b*) is defined as the absolute value of the negative suction velocity at the $(X/D, Y/D) = (0, 0)$ location. The turbulence level is about 1.0% of the time-averaged suction speed U_s. The non-uniformity of suction in the spanwise Z-direction is less than 2% of the time-averaged suction speed.

The flow is visualized by using hydrogen bubbles. The velocity measurements are obtained by a one-component DANTEC 55X laser Doppler anemometer (LDA) system. The system is set up in forward scatter mode and equipped with a Bragg cell frequency shifter for reversing flow detection. The water channel is seeded with fluorescent coated plastic particles with sizes ranging from 20 to 50 μm. The scattered light from the particles passing through the measuring volume is received by a photo-multiplier tube (PMT). The PMT signals are analysed by a TSI IFA550 frequency analyser.

The entire LDA optical system is mounted on a three-dimensional traversing mechanism, which is controlled by an 80386 personal computer. The analog output of the TSI IFA550 frequency analyser is digitized by a Data Translation DT2801A analog-to-digital (A/D) converter. The fastest digitizing rate is 27.5 kHz. In all cases, the digitizing frequency is about two orders of magnitude higher than the vortex shedding frequency. Before the experiments, two-dimensional flow was verified by looking at the time-averaged mean flow at several spanwise locations $Z/D = 5$, 10 and 15 in the Reynolds number range of the present study. The instantaneous velocity profile most likely will not be two-dimensional: Barkley & Henderson (1996) have shown that three-dimensional disturbances are absolutely unstable for Reynolds number larger than 188.5. However, the present experiment shows that the observed phenomena can be represented by two-dimensional analysis. The U and V velocities (figure 1) are measured by rotating the LDA system by 90°. By measuring the U and V velocities in the centre horizontal ($Z/D = 10$) plane with very fine grids, the spanwise vorticity, ω_z, is obtained by the difference of $\partial V/\partial X$ and $\partial U/\partial Y$ whereby the partial derivatives are calculated from the central difference of the U and V time-averaged velocity fields.

A forcing device consisting of a rod and a vibrator is used to investigate the stability of the wake flow. The forcing device vibrates the rod (diameter $d = 1.0$ mm)

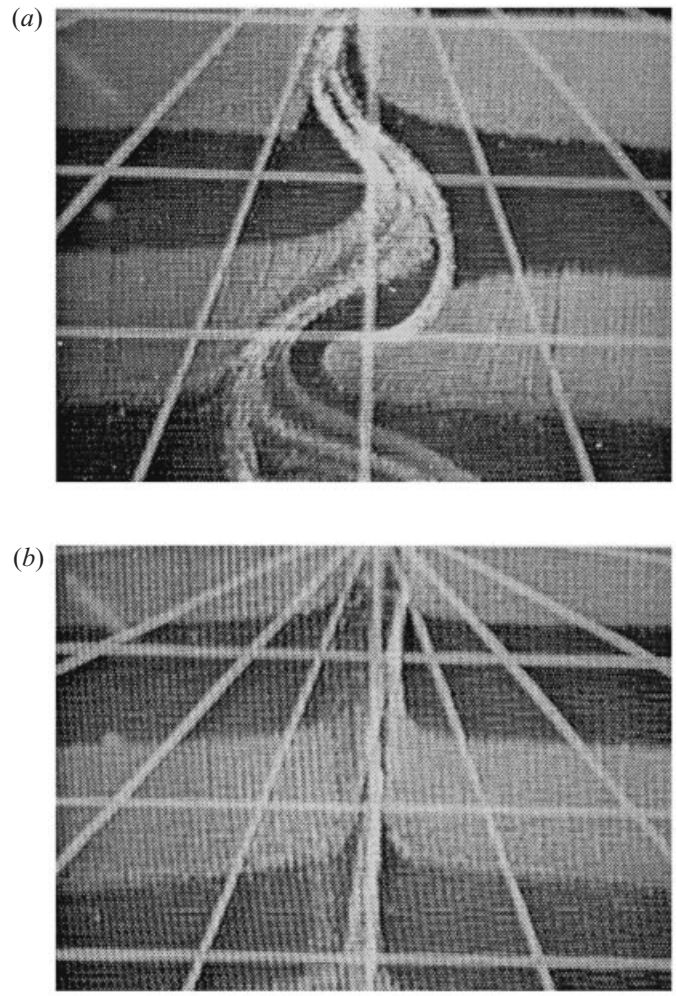

FIGURE 2. (*a*) Vortex shedding behind a flat plate with blunt base $D = 1.0\,\text{cm}$, and (*b*) suppression of vortex shedding behind the flat plate with base suction speed $U_s/U_\infty = 0.5$. $Re = 650$ or $U_\infty = 6.5\,\text{cm}\,\text{s}^{-1}$.

periodically with a sinusoidal motion. The control rod is placed at the neutral position location of $X/D = 0.5$, $Y/D = 0$. The phase of the control rod is determined by the output of a phase indicator. The phase indicator consists of a magnetic micro switch (Honeywell 3AV2C) and a ferrous vane blade. The vane blade rotates with the stepping motor. The stepping motor is controlled by an 80286 personal computer. The computer sends the desired number of pulses in an exact time period. Therefore, the frequency of the oscillating rod and the number of oscillating cycles can be controlled.

3. General features of a wake with suction

3.1. *Flow visualization*

The wake flow controlled by suction is first examined by hydrogen bubble flow visualization in the water channel. The bubbles serve as flow tracers convected in the

streamwise direction, which is from top to bottom in figures 2(*a*) and 2(*b*). When suction is not applied, the two streams merge at the trailing edge of the splitter plate. The flow is unstable due to the velocity shear. A Kármán vortex street can be observed in figure 2(*a*). Here, the Reynolds number based on the free-stream velocity, U_∞, and the width of the suction slot, D, is about 650. After the suction is applied, the flow is still unstable at low suction speeds. When the suction speed, U_s, increases and reaches a threshold level, a different type of wake flow occurs; the periodic vortices are not observed (figure 2*b*). The stable wake flow seems to persist in the streamwise direction. The suction speed at which the wake flow can be stabilized is defined as the threshold suction speed, U_{Ts}, and it equals about one half of the free-stream speed of the wake flow (Leu & Ho 1993). The statistical way of defining U_{Ts} will be discussed in § 5.

3.2. *Velocity signals*

Figure 3 displays the time traces of the streamwise velocity inside the shear layer at the location $X/D = 5.0$, $Y/D = 1.0$ for four different suction speeds. In the wake flow without suction, the velocity time trace (figure 3*a*) shows an almost periodic sinusoidal wave pattern which corresponds to the passage of vortices. As a suction speed $U_s/U_\infty = 0.24$ is applied at the trailing edge of the splitter plate, the velocity time trace (figure 3*b*) still shows similar periodic fluctuations but not as regular. As long as the suction speed U_s is less than the threshold, U_{Ts}, the flow is periodic in time. However, once the suction speed U_s/U_∞ is greater than the threshold, e.g. $U_s/U_\infty = 0.68$ (figure 3*c*), the time trace shows an almost constant velocity. The signal indicates that the flow becomes globally stable, which confirms the flow visualization results.

From the spectrum in an unstable wake flow, the dominant frequency, i.e. the frequency with the highest amplitude in the energy spectra represents the vortex shedding frequency in the wake flow (figure 4). When the suction speed is higher than the threshold velocity, $U_s > U_{Ts}$, the flow is stabilized. However, the background noise in the water channel still produces disturbances to drive the flow. This is clear from the velocity trace shown in figure 3(*c*), which displays the intermittent disturbances. The spectra (figure 4) are broadband due to the intermittent pulse-type fluctuations.

3.3. *The role of a stabilizing rod*

We found that a thin rod with diameter 1.0 mm placed within the recirculation zone is able to further stabilize the wake flow. The effects of the thin rod are demonstrated by the velocity trace (figure 3*d*) and the energy spectra (figure 4). The flow becomes very stable and the velocity remains constant for all time when the stabilizing rod is placed near the centre ($(X/D, Y/D) = (0.5, 0)$) of the recirculation region. The spectrum is at least two orders of magnitude lower than the case without a stabilizing rod at the same suction speed. The almost flat energy spectrum indicates that the disturbances have been reduced to the electronic noise level associated with the instrument.

Without the rod, appropriate base suction already can globally stabilize the wake flow. The stabilizing rod is very helpful since most of the experiments in the absolute/convective instability studies suffered from the signal-to-noise ratio problem. Continuous background noise creates difficulty in identifying a fluid system as either an absolute or convective instability. The control rod enables us to identify a flow system in a very 'clean' environment.

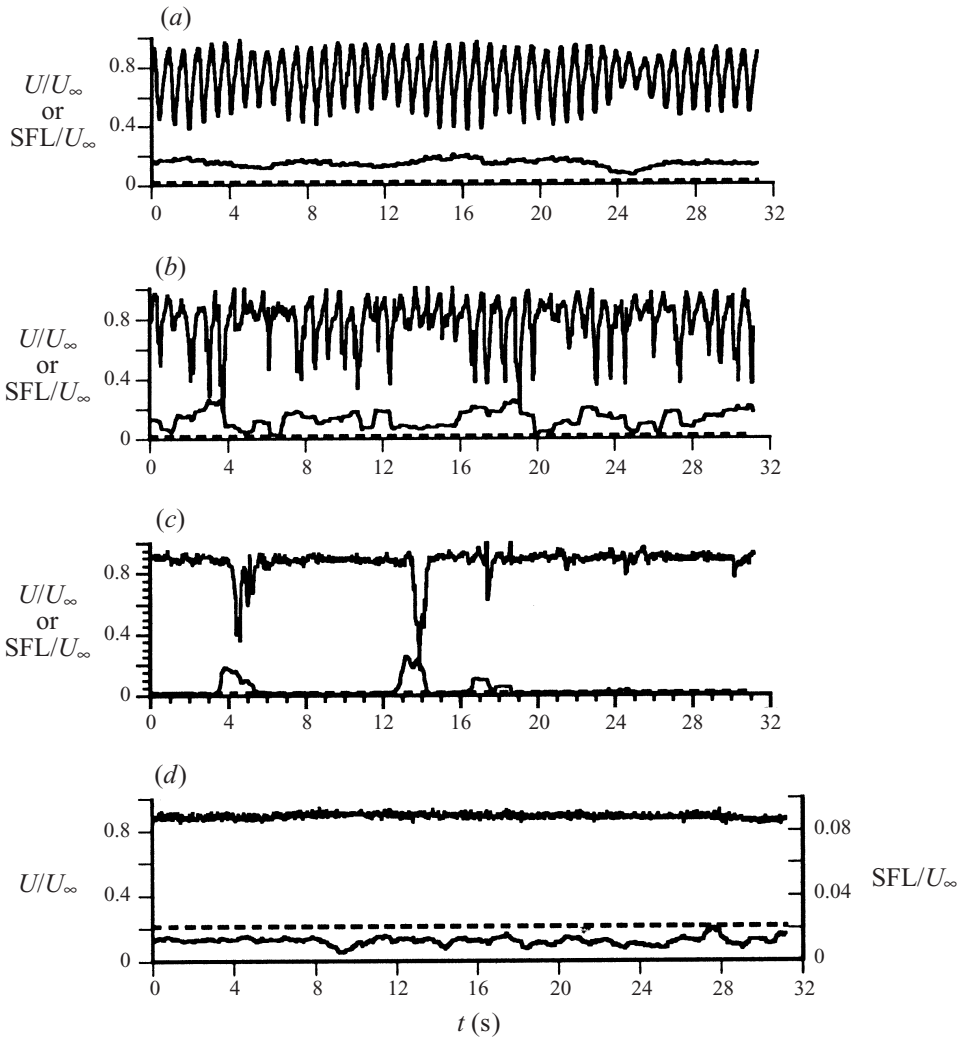

FIGURE 3. LDA velocity time trace and the short-time-averaged fluctuation level (SFL) at $(X/D, Y/D) = (5.0, 1.0)$ behind the flat plate for $Re = 1400$ and varying base suction: (*a*) $U_s/U_\infty = 0$, (*b*) $U_s/U_\infty = 0.24$, (*c*) $U_s/U_\infty = 0.68$, (*d*) $U_s/U_\infty = 0.74$ with a control rod (diameter $d/D = 0.1$) place at $(X/D, Y/D) = (0.5, 0)$. The dashed line is the value of the critical reference velocity U_{rc} in § 5.1.

4. Velocity field of the near wake

4.1. *The flow reversal region*

In free shear flows, the streamwise development is very sensitive to the initial conditions (Ho & Huerre 1984). In the present case, the suction certainly affects the flow near the origin and therefore changes the global features. In this section, the time-averaged streamwise and transverse velocity components, U and V, in the near field of the suction slot are reported. Velocity components at 900 survey stations in the centre horizontal ($Z/D = 10$) plane of the water channel were obtained by LDA. The velocity vectors in the case of a wake flow of free-stream velocity $U_\infty = 10.0\,\mathrm{cm\,s^{-1}}$ with threshold suction, $U_s/U_\infty = 0.5$, are shown in figure 5. The Reynolds number is

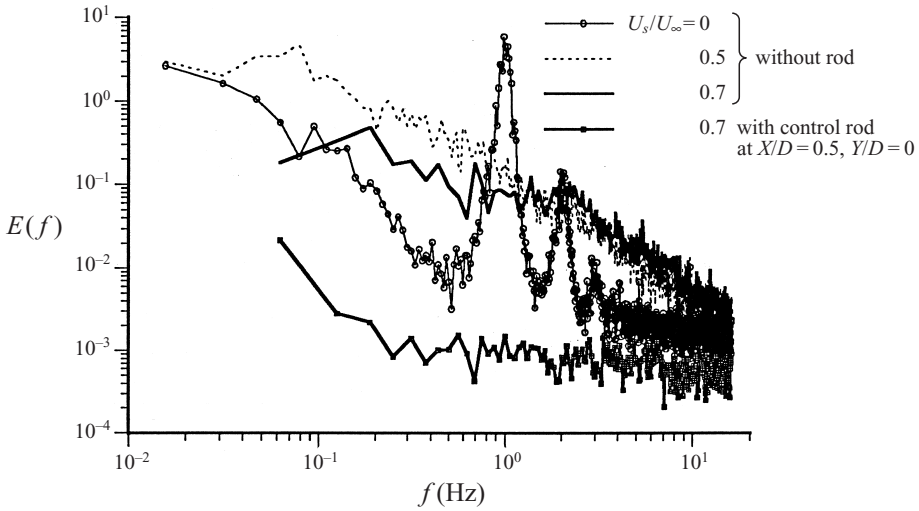

FIGURE 4. Energy spectra of velocity fluctuations at $(X/D, Y/D) = (4.0, 0.5)$ behind the flat plate with blunt base width $D = 1.0\,\text{cm}$ for $Re = 1000$ ($U_\infty = 10.0\,\text{cm s}^{-1}$) and varying base suction.

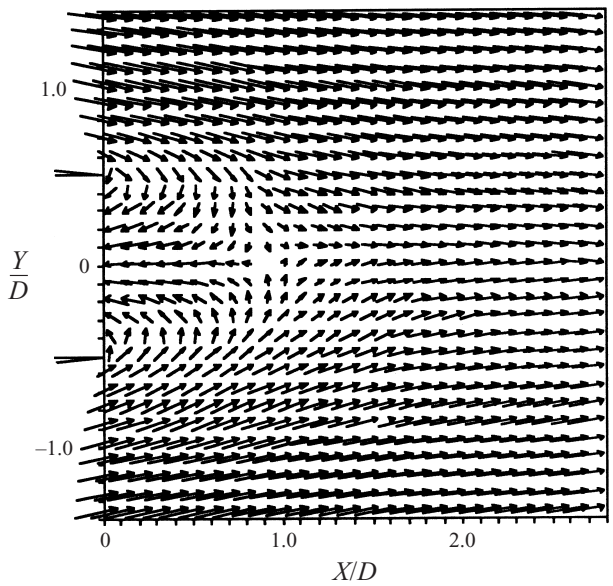

FIGURE 5. Velocity vectors behind the flat plate with base suction speed $U_s/U_\infty = 0.5$ and $Re = 1000$, $U_\infty = 10.0\,\text{cm s}^{-1}$.

about 1000. The two arrow marks at −5.0 mm and 5.0 mm on the Y-axis indicate the suction slot location. A region of reversed flow extending approximately 1.0 cm from the trailing edge is observed. Inside the flow reversal region, two standing eddies are present. By using the U and V velocities in figure 5, one can calculate the streamlines by a mass balance. The corresponding streamlines are plotted in figure 6. A saddle point was found in the streamline pattern. The dividing streamline which separates the reversed flow region from the outer flow region shows that the fluid is being sucked into the slot from a region approximately 3.0 mm in thickness each side of

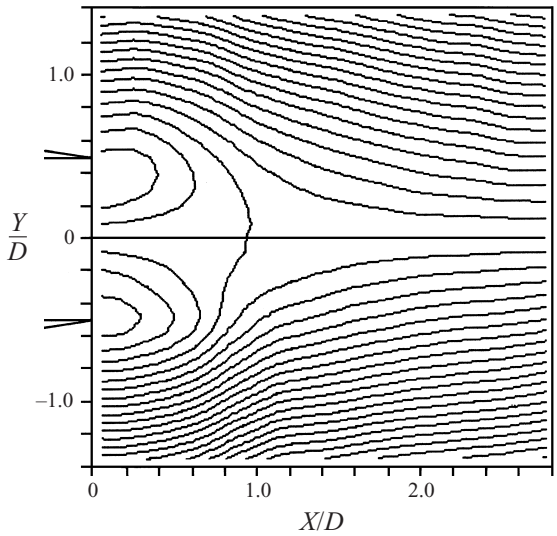

FIGURE 6. Streamline pattern of the wake flow behind a flat plate with base suction speed $U_s/U_\infty = 0.5$ and $Re = 1000$, $U = 10.0\,\mathrm{cm\,s^{-1}}$. It was computed by a mass balance from the velocity flow field shown in figure 5.

the slot. A strongly two-dimensional ($V \neq 0$) flow around the saddle point can be seen. This feature raises a concern about the validity of the parallel flow assumption ($\mathrm{d}U/\mathrm{d}X = V = 0$) used in the local stability analysis. Hence, non-parallel flow effects have to be considered in the present studies.

4.2. *The location of the saddle point*

A reversed flow region suggests the existence of an absolute instability in the wake flow (Huerre & Monkewitz 1985, 1990). The extent of the absolutely unstable region can be approximately indicated by the distance from the suction slot to the saddle point. The position of the saddle point is obviously a function of the suction speed. However, the method used in figures 5 and 6 for determining the saddle point position is cumbersome. Since the wake flow velocity profile is symmetric, an alternative method can be used. The streamwise velocity distributions along the centreline ($Y/D = 0$) of the wake with free-stream velocity $U_\infty = 10.0\,\mathrm{cm\,s^{-1}}$ are shown in figure 7. A typical centreline distribution is a negative velocity region followed by a positive velocity region. The zero crossing point is the saddle point location. At zero suction, the negative velocity is very small and the saddle point is located about 30 mm downstream from the suction slot. When the suction speed is increased, the centreline velocity changes from a negative value to a positive value within a short distance. The zero crossing point, i.e. the saddle point, moves closer to the trailing edge. The locations of the saddle points at different suction velocities, are shown in figure 8. As the suction is applied, the change in the saddle point location is very large. When the suction is close to the threshold speed, the position of the saddle point is about one slot width downstream from the suction slot. For further increase in the suction speed, the position of the saddle point moves upstream but at a much slower rate.

Since the position of the saddle point can approximately represent the length of the absolutely unstable region, the actual length of the absolutely unstable region will be slightly larger than the recirculation zone length. For details see § 5.2. The absolutely unstable region will reduce its size with the increase of suction. Chomaz, Huerre &

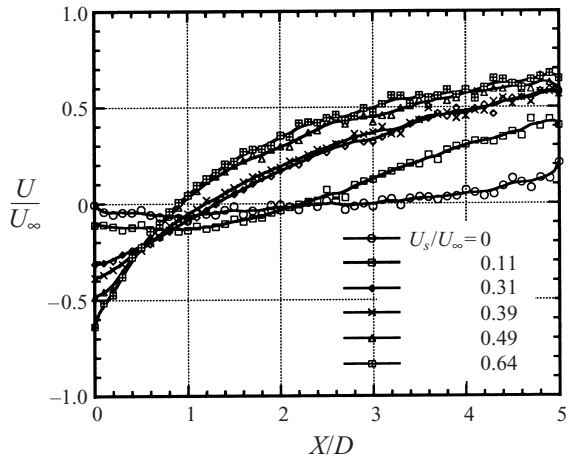

FIGURE 7. Streamwise velocity distribution along the centreline ($Y/D = 0$) at different suction speeds and $Re = 1000$, $U_\infty = 10\,\mathrm{cm\,s^{-1}}$.

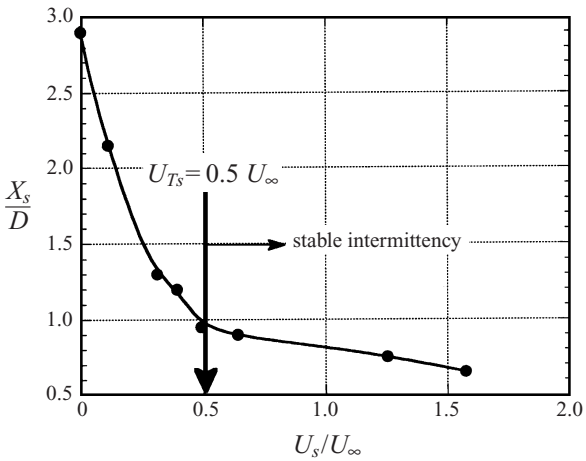

FIGURE 8. Saddle-point locations of the plane wake with different base suction speeds ($Re = 1000$, $U_\infty = 10.0\,\mathrm{cm\,s^{-1}}$).

Redekopp (1990) suggested that the absolute instability region must have a sufficient size in order to sustain a global unstable mode. Therefore, it is plausible that the absolutely unstable region may be reduced in such a way that the global mode may no longer exist. On the other hand, the temporal growth rates of streamwise velocity profiles will increase with increasing suction. Whether global instability will exist or not depends on the relative effects of these two factors.

4.3. *Inflow boundary layer profiles*

The streamline pattern in figure 6 shows that most of the fluid sucked into the slot comes from a thin layer near the solid boundary. This suggests that the boundary layer must be significantly modified by the suction process. Furthermore, the vorticity that drives the instability resides almost entirely inside the layer. Therefore, it should be interesting to investigate the effects on the inflow boundary layers caused by the suction.

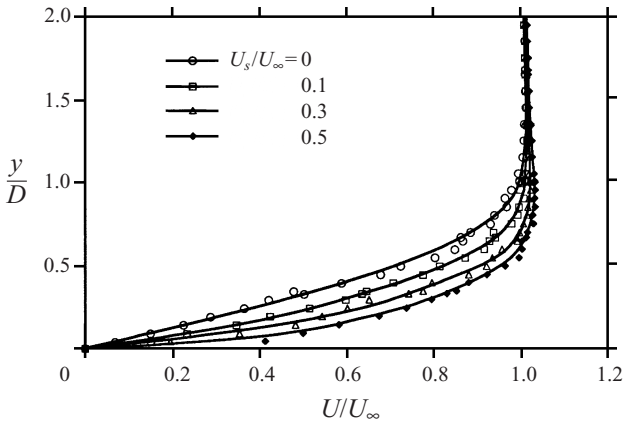

FIGURE 9. Boundary layer velocity profiles at the separation point on the trailing edge of the splitter plate with varying base suction for $Re = 1600$, $U_\infty = 16.0\,\mathrm{cm\,s^{-1}}$.

Time-averaged boundary layer velocity profiles right at the separation point on the trailing edge of the splitter plate were measured at four different suction speeds and are shown in figure 9. The boundary layer velocity profile without suction is first compared with the Blasius boundary layer velocity profile. The comparison confirms that no streamwise gradients exist in the free stream when the suction is turned off. The velocity inside the boundary layer is increased by the suction as compensation for the mass depletion through the suction slot. The distribution of the additional velocity caused by suction can be obtained by subtracting the boundary layer velocity profile without suction from the boundary layer velocity profiles with suction. Wall-jet-type velocity profiles are observed (figure 10*a*). The transverse region affected by the suction extends to about twice the thickness of the natural boundary layer thickness. These wall-jet-type profiles (Schlichting 1979) can be collapsed into a non-dimensional curve (figure 10*b*). The velocity scale used in the non-dimensional plot is the maximum velocity, U_{max}, in the wall-jet-type profile. The transverse length scale, $Y_{max/2}$, is the distance between the wall and the position where the velocity equals one half of U_{max}. Therefore, the boundary layer velocity profile with suction can be decomposed into the zero-pressure-gradient Blasius velocity profile and the wall jet profile under the favourable pressure gradient caused by the suction.

4.4. *The vorticity field*

The instability in a velocity shear region is mainly driven by vorticity. It is thus interesting to know how the vorticity distribution is affected by the suction. Based upon the time-averaged velocities, U and V, at the threshold suction speed in figure 5, it is easy to obtain the time-averaged vorticity field. The vorticity distribution and the streamline pattern are plotted together in figure 11. The magnitude of the vorticity represented by the greyscale bar is normalized by the free-stream velocity U_∞ and the width of slot D. It is evident that the region with the highest vorticity is located inside the dividing streamlines (figure 11). Since all of the vorticity which drives the instability is produced at the solid walls if there is a pressure gradient, it is easy to calculate the vorticity production from the boundary layer velocity profiles in figure 9. In figure 6, it is also noticed that the vorticity-contaminated fluid in the boundary layer will be removed by the suction. Following this idea, one may postulate that the stable wake with threshold suction can be described as the balance of vorticity production

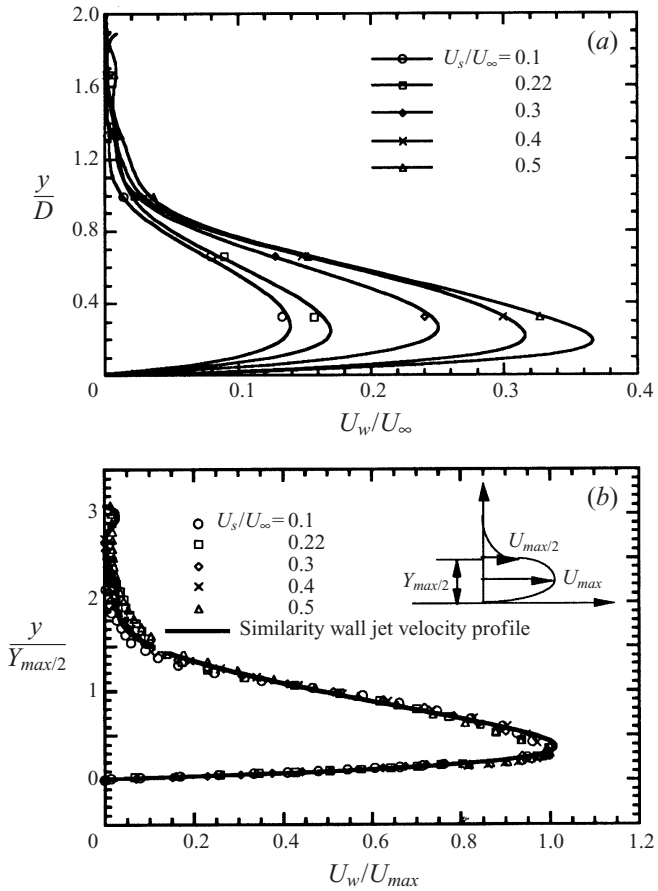

FIGURE 10. (*a*) Wall jet profiles, obtained by subtracting the Blasius velocity profile from the boundary layer profiles at different suction speeds ($Re = 1600$, $U_\infty = 16.0\,\mathrm{cm\,s^{-1}}$). (*b*) Self-similar wall jet profile after the non-dimensionalization by U_{max} and $Y_{max/2}$.

on the solid walls and its removal by the suction. To illustrate this postulation, the residual vorticity ratio is defined as

$$\text{Residual vorticity ratio} = \frac{\left[\begin{array}{c}\text{Vorticity outside the diving streamline}\\ \text{in the wake flow with suction } U_s\end{array}\right]}{\left[\begin{array}{c}\text{Vorticity production in the boundary layers}\\ \text{of an unstable wake when } U_s/U_\infty = 0\end{array}\right]}.$$

The residual vorticity outside the dividing streamline starts to decrease from 100% to about 20% of the vorticity contained in the initial boundary layers of the wake flow without suction, when the suction speed reaches the threshold level (figure 12).

5. The threshold suction speed and global stability

5.1. *Quantitative determination of the threshold suction speed*

Based upon flow visualization and the velocity traces (figures 2*a*, *b* and 3), the wake becomes stable when the suction velocity is higher than about half of the free-stream

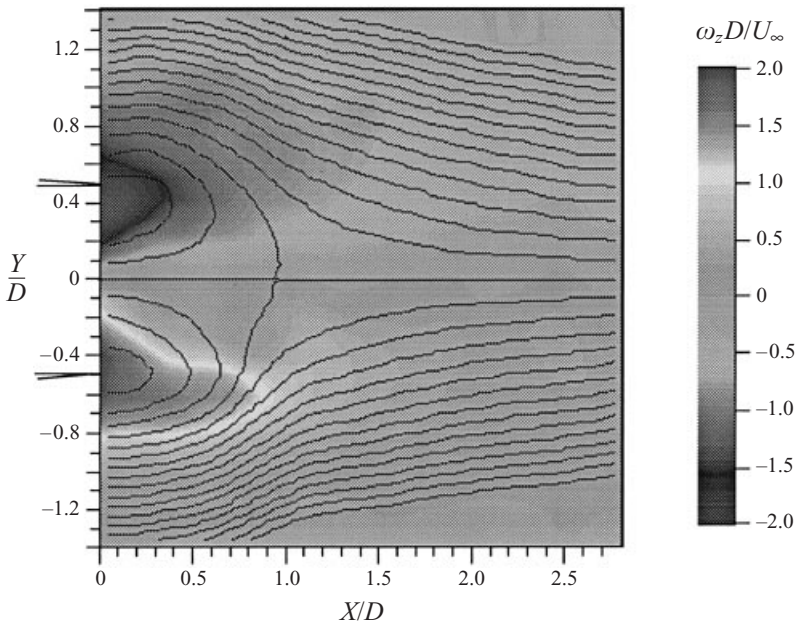

FIGURE 11. Non-dimensional vorticity distribution and streamline pattern behind the flat plate with base suction $U_s/U_\infty = 0.5$ ($U_\infty = 10.0\,\mathrm{cm\,s^{-1}}$, $D = 1.0\,\mathrm{cm}$, $Re = 1000$). The spanwise vorticity, ω_z, is obtained from the difference of $\partial V/\partial X$ and $\partial U/\partial Y$ where the partial derivatives are calculated from the central difference of the U and V time-averaged velocities in figure 5.

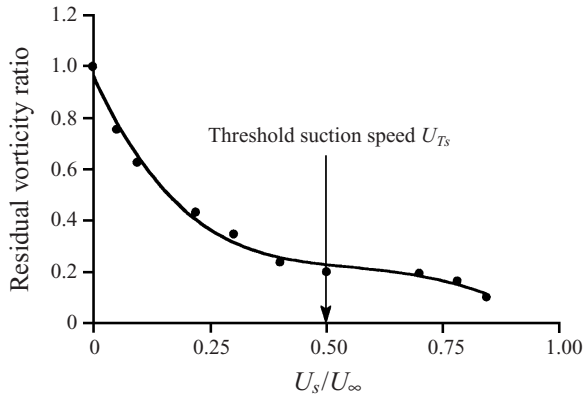

FIGURE 12. Residual vorticity ratio (vorticity outside the dividing streamline/toal vorticity at $U_s/U_\infty = 0$) at different suction speeds and $Re = 1600$, $U_\infty = 16.0\,\mathrm{cm\,s^{-1}}$.

velocity. Here, we will establish a quantitative definition for the threshold suction speed.

Figure 3(*a–d*) displays the time traces of streamwise velocity at the location $X/D = 5.0$, $Y/D = 1.0$ with free-stream velocity $U_\infty = 14.0\,\mathrm{cm\,s^{-1}}$ (Re =1400). The velocity traces change from a continuous periodic signal to an intermittent spiky fluctuation and finally to an almost constant value as the suction increases. A method to determine the threshold speed from the intermittent nature of the signal was developed. A short time-averaged fluctuation level (SFL) of the velocity signal similar to the VITA signal

processing scheme (Blackwelder & Kaplan 1976) is defined as

$$\mathrm{SFL}(t) = \left\{ \frac{1}{T} \int_t^{t+T} [U(\tau) - \hat{U}(\tau)]^2 \, \mathrm{d}\tau \right\}^{1/2}. \tag{1a}$$

Note that T is the period of the vortex shedding when $U_s/U_\infty < 0.5$ or the period of the vortex shedding without suction when $U_s/U_\infty \geqslant 0.5$, and $\hat{U}$ is a short time-averaged velocity, defined as

$$\hat{U} = \frac{1}{T} \int_t^{t+T} U(\tau) \, \mathrm{d}\tau. \tag{1b}$$

The profile of SFL(t) clearly indicates the intermittency of the signal. In figures 3(*a–c*), the time trace signal changes from sinusoidal to intermittent and finally to an almost constant value as the suction increases. The SFL(t) for figures 3(*b*) and 3(*c*) shows the intermittent feature.

The value of SFL indicates the stability of the flow. In the range tested, SFL(t) varies from about 0.7% of U_∞ (0.1 cm s^{-1} in figure 3*d*) to 28% of U_∞ (4 cm s^{-1} in figure 3*b*). In figure 3(*d*), the value of SFL(t) is much lower than that of figure 3(*a–c*). Note that the scale of the SFL signal is plotted on the right-hand side of figure 3(*d*). The probability of SFL(t) being less than a reference value is defined as

$$P(U_r) = \mathrm{Prob}\,(\mathrm{SFL} \leqslant U_r) = \lim_{\hat{T}\to\infty} \frac{\sum_{i=1}^{k} \Delta t_i}{\hat{T}}, \tag{2a}$$

where Δt_i is the time interval in which SFL $\leqslant U_r$. A long time history record ($\hat{T} = 10\,240$ cycles) is used in this experiment. The probability distributions at various suction speeds are shown in figure 13. When the value of U_r changes from 0 to 4 cm s^{-1}, $P(U_r)$ increases from 0 and approaches 1. When the stabilizing rod is not there (the 'without rod' cases in figure 13), the probability of high velocity fluctuation signals ($U_r > 2.0$ cm s^{-1}) increases with increasing suction speed from $U_s/U_\infty = 0$ to 0.24. This indicates that at this Reynolds number small suction favours instability. The velocity time trace in figure 3(*b*) or in the linear global growth rates in figure 19 below seem to support this statement. As soon as $U_s/U_\infty \geqslant 0.49$, the probability of low velocity fluctuation signals ($U_r < 2.0$ cm s^{-1}) starts to increase. For example, $P(U_r = 1.0\,\mathrm{cm\,s^{-1}})$ increases to 40% at $U_s/U_\infty = 0.49$ and 70% at $U_s/U_\infty = 0.69$ in figure 13.

A critical reference velocity U_{rc} is defined as the minimum value of reference velocity U_r at different suction speeds at which probability distribution functions $P(U_r)$ reach their asymptotic value. In other words, the value of U_{rc} represents a background velocity fluctuation reference at the measuring point $(X/D, Y/D) = (5.0, 1.0)$ within the stable wake. When the stabilizing rod is used (the 'with rod' cases in figure 13), the critical reference velocity U_{rc} is found to be $U_{rc} = 0.3$ cm s^{-1} (or $U_{rc}/U_\infty = 2.1\%$) and remain constant in the stable wake flow as long as the suction speed is higher than 70% of the free-stream velocity (see $U_s/U_\infty = 0.7$ and $U_s/U_\infty = 0.74$ cases in figure 13). Hence, $U_{rc} = 0.3$ cm s^{-1} or $U_{rc}/U_\infty = 2.1\%$ is taken as a stringent criterion that represents the background velocity fluctuation for determining whether the wake is stable or not. We define a stable intermittency function $I(U_s/U_\infty)$ based on U_{rc} which measures the percentage of time in which the wake is stable:

$$I\left(\frac{U_s}{U_\infty}\right) = \mathrm{Prob}\left[\mathrm{SFL}(t) \leqslant \frac{U_{rc}}{U_\infty} = 2.1\%\right] = \lim_{T\to\infty} \frac{\sum_{i=1}^{k} \Delta t_i}{\hat{T}}, \tag{2b}$$

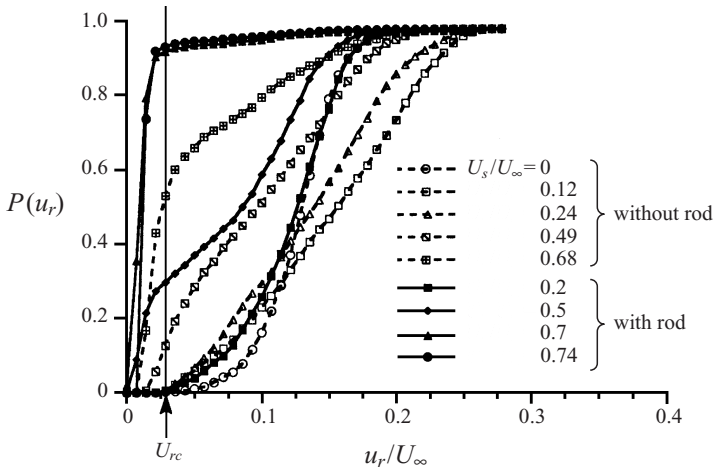

FIGURE 13. Cumulative probability distribution function $P(U_r)$ of the velocity trace measured at $(X/D, Y/D) = (5.0, 1.0)$ with varying suction speeds and $Re = 1400$. The corresponding velocity traces have been partially shown in figure 3.

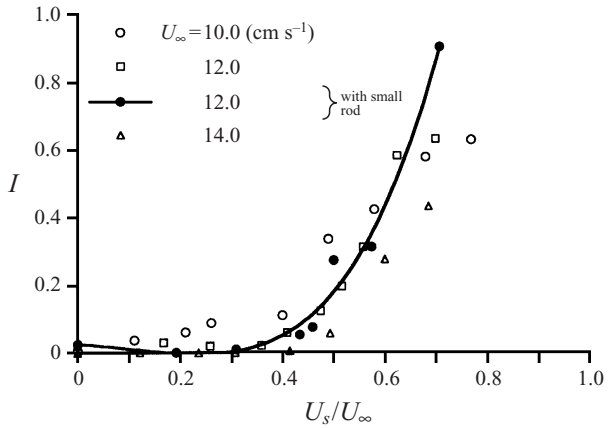

FIGURE 14. Stable intermittency I as function of suction speed (U_s/U_∞) at free-stream velocities $U_\infty = 10\,\mathrm{cm\,s^{-1}}$ $(Re = 1000)$, $U_\infty = 12\,\mathrm{cm\,s^{-1}}$ $(Re = 1200)$, and $U_\infty = 14\,\mathrm{cm\,s^{-1}}$ $(Re = 1400)$.

where Δt_i is the time interval in which $\mathrm{SFL}(t) \leqslant U_{rc}$. If the value of $I(U_s/U_\infty)$ is high, it means that the value of SFL is low and the wake is stable. A sharp rise of $I(U_s/U_\infty)$ is observed as the suction speed reaches 50% of the free-stream velocity in figure 14, which confirms the flow visualization results (figure 2*b*). This suction speed is defined as the threshold suction speed, U_{Ts}.

5.2. *Local stability analysis*

To gain a deeper understanding of the wake stabilized by suction, it should be helpful to do a hydrodynamic stability analysis. In principle, the linear hydrodynamic stability analysis in a shear flow starts with a base flow, which mathematically is the solution of the steady flow equations. One then considers this solution with perturbation superimposed, and enquires whether this perturbation grows or decays in time. For linear analysis, the amplitude of perturbations is limited to low level. A time-averaged velocity profile for local analysis is appropriate. The other issue is the viscous effect.

Monkewitz (1988) investigated the effect of viscosity on the hydrodynamic instabilities in the low-Reynolds-number two-dimensional wake flow. He calculated the stability characteristics in the wake flow by using measured time-averaged velocity profiles behind a cylinder and found that the flow is practically inviscid when the Reynolds number is higher than 100. The definition of Reynolds number in the work by Monkewitz is based on the average mean velocity $U_{1/2} = (U_{Y=0} + U_\infty)/2$ and local half-width $b_{1/2}$ of the wake, which is defined by $U(b_{1/2}) = U_{1/2}$. In the present experiments, the range of Reynolds number (based on the same velocity scales $U_{1/2}$ and length scale $b_{1/2}$) is from 150 to 650. Therefore, the inviscid Rayleigh equation is adequate:

$$\left(U - \frac{\omega}{k}\right)\left(\frac{\mathrm{d}^2\Phi}{\mathrm{d}y^2} - k^2\Phi\right) - \frac{\mathrm{d}^2U}{\mathrm{d}y^2}\Phi = 0, \tag{3}$$

where $U(y)$ is the steady-state mean velocity profile, ω is frequency, k is wavenumber, and Φ is defined in the form of the normal modes of the perturbation stream function

$$\Psi(x, y, t) = \Phi(y)\mathrm{e}^{\mathrm{i}(kx-\omega t)}.$$

The Rayleigh equation (3) involves the second derivative of the mean velocity profile. Thus, an accurate fit of the velocity profile is critical. Here, the experimentally measured velocity profiles are curve-fitted with a two-parameter (R, N) equation (Monkewitz & Nguyen 1987)

$$U(y) = 1 - R + 2RF(y), \tag{4a}$$

where

$$R = \frac{U_{Y=0} - U_\infty}{U_{Y=0} + U_\infty}, \tag{4b}$$

$$F(y) = [1 + \sinh^{2N}(y \sinh^{-1} 1)]^{-1}. \tag{4c}$$

Note that $U_{Y=0}$ is the dimensional velocity at the location $Y = 0$ and the terms in (4*a*) are made non-dimensional with average mean velocity $U_{1/2} = (U_{Y=0} + U_\infty)/2$ and local half-width $b_{1/2}$ of the wake, which is defined by $U(b_{1/2}) = U_{1/2}$. The mean velocity profiles for the wake flow at $Re = 1600$ with varying suction speeds $U_s/U_\infty = 0$, 0.19, 0.4, 0.5 and 0.62 are surveyed at several downstream locations and shown in figure 15. To determine the best fitting two-parameter (R, N) equation for the velocity profiles in figure 15, the average mean velocity $U_{1/2}$ and local half-width $b_{1/2}$ of the wake are used to non-dimensionalize the measured velocity profiles. The value of parameter R can be easily decided from $U_{Y=0}$ and U_∞ in (4*b*). Different values of N are chosen to curve fit the non-dimensional velocity profile such that the standard deviation between the non-dimensional velocity profile and two-parameter (R, N) equation (4) is less than 1.0% of free-stream velocity U_∞.

The best-fit parameters (R, N) at each streamwise location are listed in figure 15. In the wake flow without suction (figure 15*a*), the velocity profile starts at $N = 2.0$ and $R = -1.004$ right behind the body and approaches $N = 1.4$ and $R = -0.492$ at $X/D = 4.4$. The slightly reverse flow region (i.e. the $R < -1$ region) can be seen between $X/D = 0$ and 2.4. In the wake with suction (figure 15*b–e*), the profiles are all bell-shaped and the shape parameter N does not change very much. The typical values are between $N = 2.0$ just behind the trailing edge and $N = 1.0$ further downstream. A large decrease in the value of R at the initial velocity profiles from $R = -1.435$ (figure 15*b*) to $R = -4.061$ (figure 15*e*) can be seen and indicates the increasingly reversed flow due to the increasing suction.

The maximum deviation between the two-parameter curve fitting and the experimental velocity profile is less than 1% in all measurements. The slight overshoot in the shoulder region of the velocity profile is the main cause of these deviations. Monkewitz (1988) studied the overshoot effects on the stability analysis. The variation of eigenvalues $|\omega_0|$ and $|k_0|$ is less than 3% for an overshoot, U_∞/U_{max}, between 1.0 and 0.85, where eigenvalues k_0 and ω_0 are the complex wavenumber with zero group velocity $((\mathrm{d}\omega/\mathrm{d}k)(k_0) = 0)$ and its corresponding absolute frequency $(\omega_0 = \omega(k_0))$ respectively. In the present case, the maximum overshoot U_∞/U_{max} is about 0.9. Therefore, the effect on the eigenvalues should be less than 3%.

The absolute frequency, ω_0, was calculated by solving the Rayleigh equation with boundary conditions

$$\begin{bmatrix} \phi \\ \phi' \end{bmatrix} (y \to \infty) = \begin{bmatrix} 1 \\ -k \end{bmatrix} \mathrm{e}^{(-ky)} \tag{5a}$$

and

$$\begin{bmatrix} \phi \\ \phi' \end{bmatrix} (y \to 0) = \begin{bmatrix} 1 \\ 0 \end{bmatrix} \quad \text{'sinuous mode'}. \tag{5b}$$

We have calculated the complex wavenumber, k_0, which has a zero group velocity $(\mathrm{d}\omega/\mathrm{d}k)(k_0) = 0$ and its corresponding absolute frequency $\omega_0 = \omega(k_0)$. The dispersion relation was found by a shooting method. For a given real k and an appropriate initial guess ω, equation (3) with boundary conditions (5) is integrated from $y = +\infty$ to $y = y_c$ and from $y = 0$ to $y = y_c$ by using a standard fourth/fifth-order Runge–Kutta scheme. If the initial guess is an eigenvalue, the solutions from both sides will match at $y = y_c$. Otherwise, the frequency ω is updated by Newton's method until the matching criterion is satisfied. Then, the saddle point $(\mathrm{d}\omega/\mathrm{d}k)(k_0) = 0$ in the complex k-plane can be found by Newton's method. The maximum principle in complex analysis, which states that the maximum and minimum must appear on the boundary, automatically excludes the possibility of finding a maximum or minimum.

In the codes for wake instability studies, the boundary condition for $y = +\infty$ is applied at the boundary $y = Y/b_{1/2} = 4.0$ since the velocity profiles in figure 15 remain unchanged when $y > 4.0$. In the present studies $y_c = Y/b_{1/2} = 1.0$ is chosen (the choice of y_c can be arbitrary in the iteration Runge–Kutta procedure). Figure 16(*a*) shows the computed results of the temporal growth rate $\omega_{0i}^{(D)}$ as a function of the streamwise coordinate, X/D, in the wake flow $Re = 1600$ at different suction speeds. The superscript (D) is used to indicate non-dimensionalization by using the free-stream velocity U_∞ and the width of the suction slot D. The location where $\omega_{0i}^{(D)}$ varies from a positive to a negative value indicates a change from absolutely unstable flow to absolutely stable flow. Figures 15 and 16(*a*) indicate that the centreline velocity does not have to be negative for absolute instability. For a typical shape parameter N, which varies from 1.0 to 2.0, the velocity profiles are absolutely unstable if the centreline velocity is less than 5% of the free-stream velocity.

The maximum temporal growth rate $\omega_{0i}^{(D)}$ becomes larger when the suction speed increases. This is expected due to the increased back flow induced by the suction. The real part of $\omega_0^{(D)}$, $\omega_{0r}^{(D)}$, at each downstream location is shown in figure 16(*b*). The maximum $\omega_{0i}^{(D)}$ as a function of the suction speed is shown in figure 17. No clear change of the trend is observed around U_{Ts}.

It is known that local absolute instability is a necessary but not a sufficient condition for global instability (Chomaz, Huerre & Redekopp 1988). Chomaz *et al.*

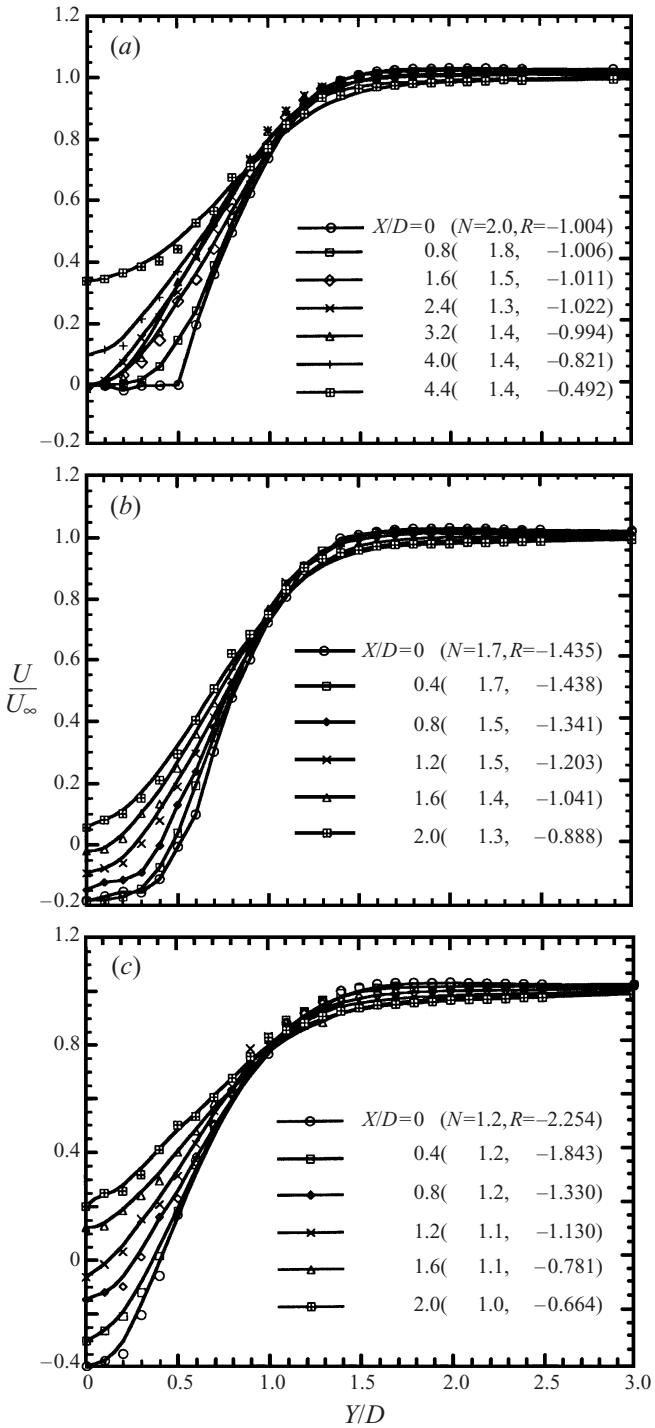

FIGURE 15. For caption see facing page.

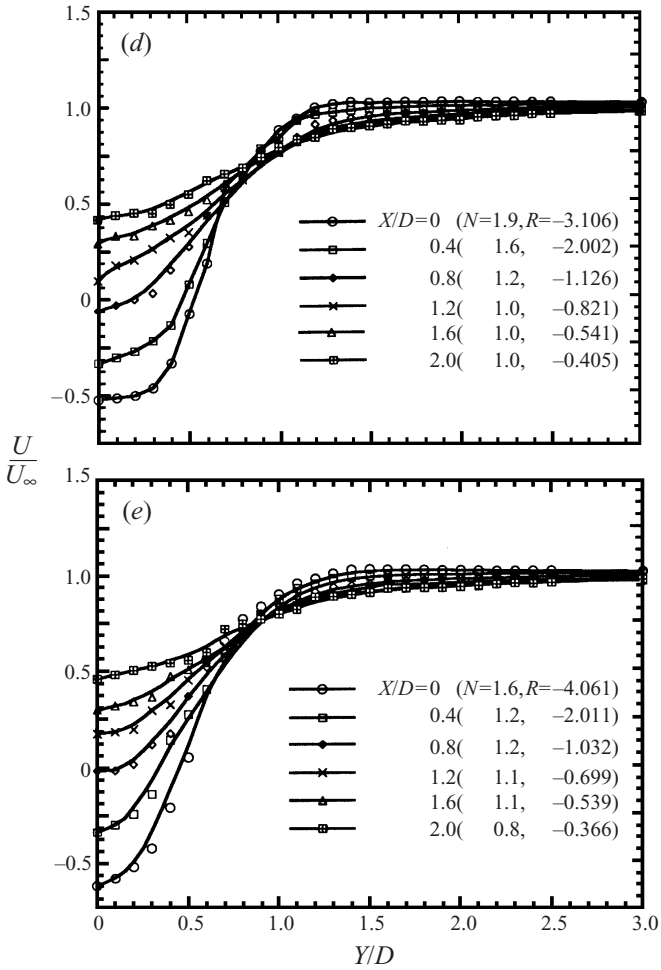

FIGURE 15. Time-averaged mean velocity profiles at different streamwise locations at (*a*) $U_s/U_\infty = 0$, (*b*) 0.19, (*c*) 0.40, (*d*) 0.50, (*e*) 0.62 ($D = 1.0\,\text{cm}$, $U_\infty = 16.0\,\text{cm}\,\text{s}^{-1}$, $Re = 1600$).

(1990) proposed a global instability criterion for slowly varying base flow:

$$\text{GIC} = \int_0^{X_a/D} \sqrt{\omega_{0i}^{(D)}}\,\mathrm{d}x \geqslant O(1). \tag{6}$$

Note that X_a is the length of the absolutely unstable region and here $\omega_{0i}^{(D)}$ is non-dimensional temporal growth rate through the use of the free-stream velocity U_∞ and the width of the suction slot D. X_a decreases with increasing suction speed (figure 16*a*). Based upon the data in figures 16 and 17, GIC is calculated and shown in figure 18. GIC smoothly decreases with increasing suction speeds. Again, there is no clear indication of a globally stable flow near U_{Ts}.

5.3. *The global instability analysis with non-parallel flow correction*

In the case of a parallel flow, the temporal frequency ω_0 should remain the same along the streamwise direction. Hence, the variations of the absolute frequency ω_0 along the streamwise direction indicate the non-parallel characteristics, especially in a wake

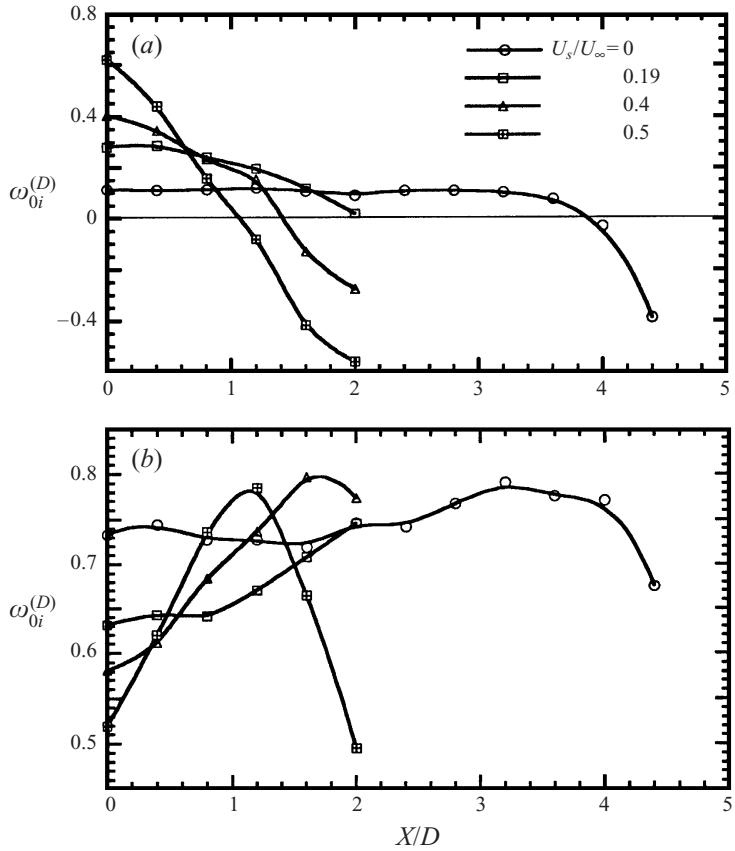

FIGURE 16. (*a*) Absolute growth rate $\omega_{0i}^{(D)}$ and (*b*) Real part of absolute frequency $\omega_{0r}^{(D)}$, as functions of X/D at different suction speeds.

with suction. In the wake flow without suction, the two parameters R and N of the mean velocity profiles at different streamwise locations in figure 15(*a*) change in such a way as to keep the absolute growth rate, ω_{0i}, constant with increasing X/D. Figure 16 shows the fairly flat distribution along the streamwise locations from $X/D = 0$ to $X/D = 3$ at $U_s = 0$. When the suction is applied at the trailing edge of the wake flow, the maximum absolute growth rate increases and the zone with constant ω_{0i} shortens. At the same time, the slopes of absolute growth rate along the streamwise direction become steeper with increasing suction speeds, i.e. the flow becomes more non-parallel with the increasing suction speed.

By applying a global linear stability analysis derived for weakly non-parallel shear flow, Monkewitz *et al.* (1993) showed that the non-parallel correction term is determined by the slope of the absolute frequency $\omega_0(X^t)$ at the dominant turning point, X^t, of the WKBJ approximation. The region around the turning point, X^t, can be viewed as a wavemaker for the entire flow field. The global frequency of the entire flow field is not locally determined but is instead determined by a region near the turning point. The global frequency, ω_G, can be split into the dominant absolute frequency $\omega_0(X^t)$, abbreviated as ω_0^t, at the turning point, X^t, i.e. the frequency of the mode with zero group velocity at turning point, X^t, and a small correction term, ω_ε, corresponding to the non-parallel effect. The global mode frequency for the

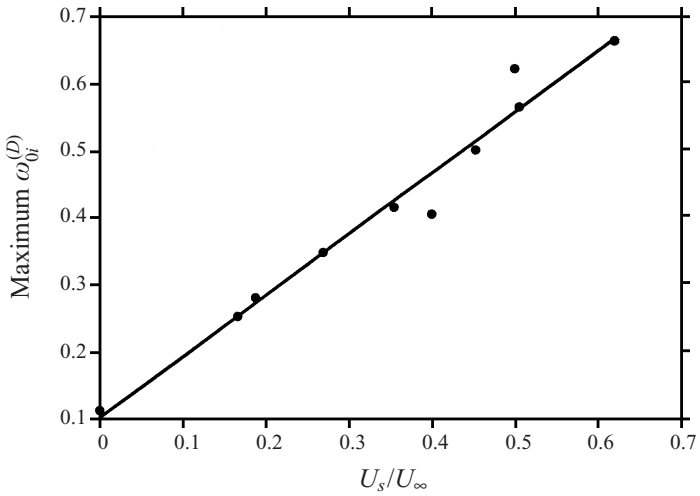

FIGURE 17. The maximum absolute growth rate as function of suction speed ($Re = 1600$).

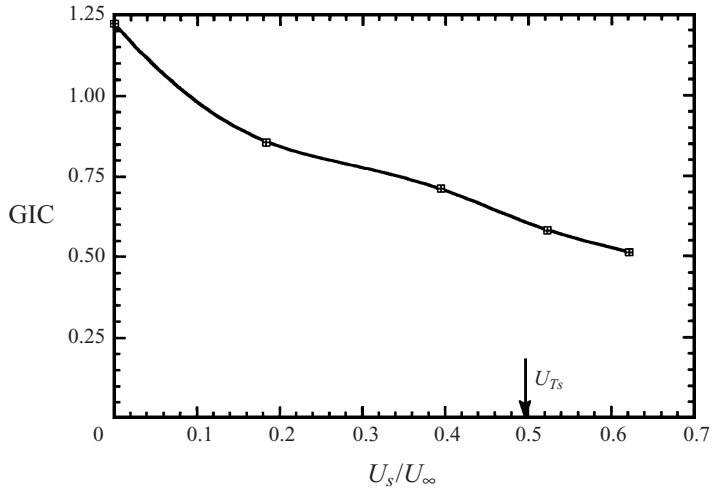

FIGURE 18. Global instability criterion (GIC) proposed by Chomaz *et al.* (1990).

non-parallel flow is given by

$$\omega_G \sim \omega_0^t + \omega_\varepsilon = \omega_0^t + \varepsilon^{2/3}\left\{\omega_X^t(2\omega_X^t/\omega_{kk}^t)^{-1/3}a_0\right\}, \tag{7a}$$

where a_0 (= 2.338) is a zero of the Airy function, the superscript t indicates the turning point X^t of the WKBJ approximation, and $X = \varepsilon x$ is the 'slow' coordinate in the terminology of the method of multiple scales (Bender & Orszag 1978). The parameter

$$\varepsilon \equiv \lambda_{typ}\{\delta^{-1}(x)[\mathrm{d}\delta/\mathrm{d}x]\}_{typ} \ll 1 \tag{7b}$$

characterizes the degree of the spatial inhomogeneity of the basic flow by providing a measure of the change of the typical cross-stream length scale $\delta(x)$ over one typical instability wavelength λ_{typ}. Monkewitz *et al.* also found that the turning point in the wake flow with suction is at the origin of the wake, $X^t = 0$. Hence, the non-parallel correction term strongly depends on the initial slope of the absolute frequency at

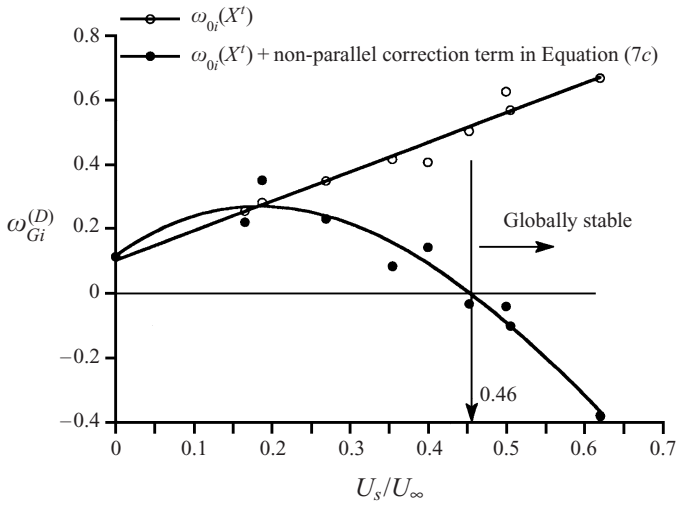

FIGURE 19. Global growth rate computed using the non-parellel correction in the wake flow with suction ($D = 1.0\,\text{cm}$, $U_\infty = 16\,\text{cm}\,\text{s}^{-1}$, $Re = 1600$).

$X/D = 0$ in figures 16(a) and 16(b). The zero initial slope of the natural wake without suction indicates that the parallel flow assumption can be applied. As the suction speed, U_s/U_∞, increases, the negative slope of the absolute growth rate $\omega_{0i}^{(D)}$ in figure 16(a) and the positive slope of $\omega_{0r}^{(D)}$ in figure 16(b) no longer remain negligible. The non-parallel correction term, ω_ε, increases significantly.

In determining the non-parallel correction term, ω_ε, equation (7a) is first re-non-dimensionalized by using the width of the suction slot D and the free-stream velocity U_∞ and becomes

$$\omega_G^{(D)} \sim \omega_0^{t^{(D)}} + a_0\{\omega_x^{t^{(D)}}(2\omega_x^{t^{(D)}}/\omega_{kk}^{t^{(D)}})^{-1/3}\}. \tag{7c}$$

In (7c), the parameter ε vanishes. The $\omega_{kk}^{t^{(D)}}$ term is the second derivative of the absolute frequency $\omega_0^{(D)}$ in the complex k-plane, which has been calculated by Newton's iteration method during the finding of the saddle point $(\mathrm{d}\omega/\mathrm{d}k)(k_0) = 0$. The $\omega_X^{t^{(D)}}$ term is the first derivative of the absolute frequency $\omega_0^{(D)}$ at the turning point $X^t = 0$ with respect to streamwise coordinate X/D which can be obtained by second-order-accurate finite difference approximation at the location $X/D = 0$ in figure 16.

For a typical mean velocity profile of the wake flow with suction in figure 15, the velocity ratio parameter R varies from $-1\,(U_s/U_\infty = 0)$ to $-4\,(U_s/U_\infty = 0.62)$; the shape parameter changes from a top-hat shape ($N = 2$) to a far-wake profile ($N = 1$). In comparison with the absolute frequency $\omega_0^{(D)}$ in figure 16 and the R and N parameters in figure 15, the absolute frequency $\omega_0^{(D)}$, especially the temporal growth rate $\omega_{0i}^{(D)}$, was found to be more sensitive to the velocity ratio parameter R than the shape parameter N. Therefore, the $\omega_x^{t^{(D)}}$ term in the non-parallel correction term of (7c) is sensitive to the change of the velocity ratio parameter R around the $X/D = 0$ region, which is defined from the velocity distribution near the suction slot. Since it is possible to measure the reverse flow near the suction slot accurately by using LDA, highly accurate and complete mean flow data are available in our stability analysis.

The results of the global growth rate through the use of (7c) are shown in figure 19. The ascending curve with open circle symbols which are all positive shows that the flow is locally absolutely unstable based upon the leading order of the global

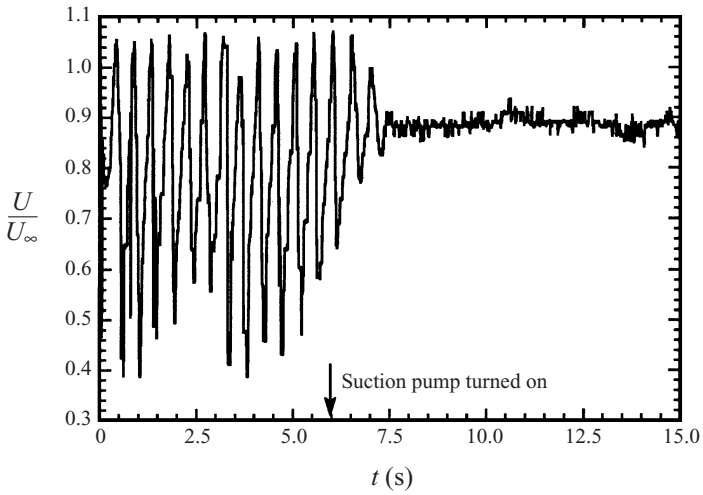

FIGURE 20. Supercritical transient of U-velocity time trace at $(X/D, Y/D) = (3.0, 0.5)$ for the plane wake flow at $Re = 1900$ with suction $U_s/U_\infty = 0.75$ turned on at $t = 6.0$ s.

growth rate at the turning point, $\omega_{0i}^{(D)}$ $(X^t = 0)$. If the non-parallel correction term is considered in (7*c*), the global growth rate changes its sign from positive to negative when the suction speed is equal to about 0.46 of the free-stream velocity. In other words, the global instability breaks down and the flow becomes stable at the suction speed equalling 0.46 of the free-stream velocity U_∞, which is very close to the threshold suction speed $0.5U_\infty$ determined experimentally (§§ 3.1 and 5.1). This study has clearly illustrated the effect of non-parallel flow on global instability.

5.4. *Self-excitation of the wake*

A wake is a flow self-excited by the oscillations produced by absolute instability. This concept can be best illustrated by a transient experiment in the present case where the absolute instability can be turned on or off through the non-parallel mechanism.

Figure 20 shows the transient behaviour in the wake flow by measuring the velocity trace at the location $(X/D, Y/D) = (3.0, 0.5)$. The non-parallel effect is not strong and the near wake is absolutely unstable so that large-amplitude velocity fluctuations exist in the flow. At the instant of $t = 6.0$ s, a supercritical suction speed (i.e. $U_s > U_{Ts}$) is switched on. In 2 s, the non-parallel flow region is established. The growth rate of the absolute instability becomes less than zero. The velocity trace changes from large-amplitude oscillations to a nearly flat signal (a thin rod placed at $(X/D, Y/D) = (0.5, 0)$ is used in this experiment to further stabilize the flow in the supercritical suction case). This experiment has clearly demonstrated that the wake flow can be globally stable if the self-excitation is 'shut off' by the non-parallel flow caused by suction in the near-wake region.

5.5. *The impulse response in a globally stable flow*

When the absolute instability region is significantly affected by the non-parallel near-wake region produced by suction, it would be interesting to examine the response of the stabilized flow to artificial perturbations. It is known that background noise can obscure an experiment involving global instabilities (Huerre & Monkewitz 1990). We therefore employed the stabilizing rod, which can significantly reduce the background noise (figure 4). At the same time, the rod can be vibrated by a driving mechanism at

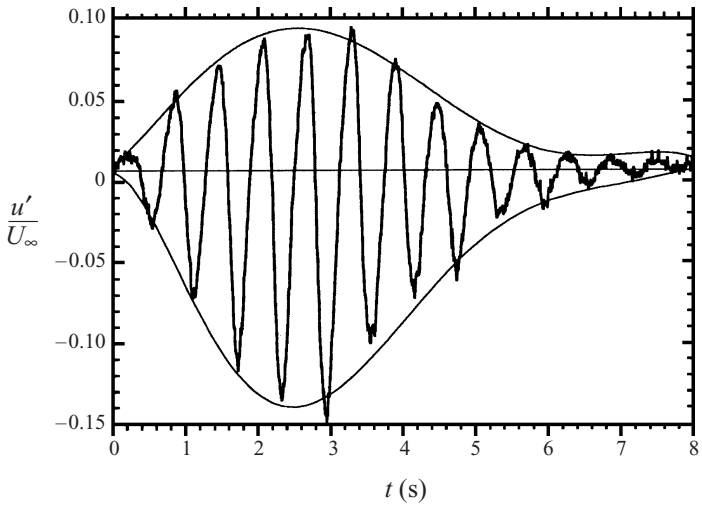

FIGURE 21. Impulse train response of U-velocity fluctuation at $(X/D, Y/D) = (3.0, 0.5)$ for the plane wake flow at $Re = 1600$ with suction $U_s/U_\infty = 0.75$ and five transverse pulses by oscillating a rod at 1.7 Hz amplitude of $0.05D$.

a chosen frequency (Leu 1994) and serve as a forcing device to provide the required perturbations.

The rod is driven in an impulse mode. Each impulse contains a train of five cycle oscillations at a frequency of 1.7 Hz, which is close to the most amplified frequency of the wake. The response of the flow system to the pulse train is measured by LDA at different streamwise locations along the $Y/D = 0.5$ line. The signal is phase-averaged. The phase reference is based on the electronic signal that drives the oscillating rod. Slight phase jitters between the phase reference and the velocity fluctuations were observed.

Figure 21 shows the pulse train response at $(X/D, Y/D) = (3.0, 0.5)$ in the wake flow at $Re = 1600$ when suction speed $U_s/U_\infty = 0.75$ (where $U_\infty = 16.0\,\mathrm{cm\,s^{-1}}$) is applied at the trailing edge. More than five cycle oscillations with non-constant amplitude are observed. This results from the combined response of the solid rod and the flow to the original driving signal. The wake is globally stable at this suction speed. Figure 22 shows the spatio-temporal evolution of the pulse train obtained along $Y/D = 0.5$ in the convective stability region. The convective nature is obvious. The convection speed is $12.5\,\mathrm{cm\,s^{-1}}$ which is 0.78 of the free-stream speed. A slight growth of the signal is shown from the first measuring station to the second station. The amplitude of the phase-averaged signal decays slowly, which is believed to be caused by the phase jitters between the driving signal and the velocity pulse train arriving at the measuring station. We therefore introduce a different technique in the following section to clarify this phenomenon.

5.6. *The convective neutrally stable flow*

For perturbations applied in a steady manner, the evolution of narrow-band energy at a specific frequency f across the velocity shear region, $E[u'(f)]$, can be used to indicate the growth or decay of the perturbations along the streamwise direction (Ho & Huang 1982). $E[u'(f)]$ is based on the spectral analysis which is not sensitive to

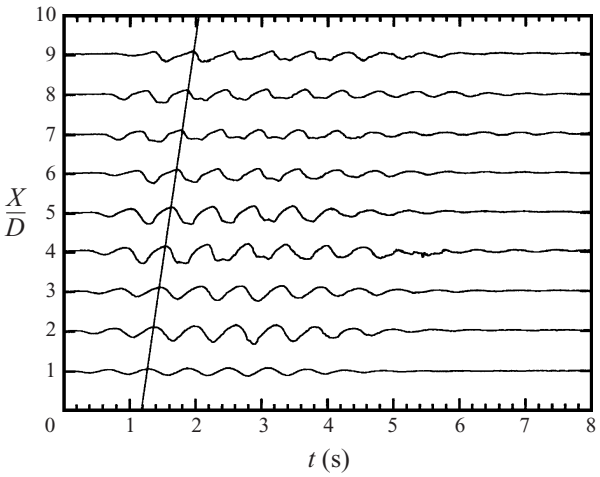

FIGURE 22. Impulse train response of U-velocity time trace at different downstream locations along $Y/D = 0.5$ in the plane wake flow at $Re = 1600$ with suction $U_s/U_\infty = 0.75$ and five transverse pulses by oscillating a rod at 1.7 Hz with amplitude of $0.05D$.

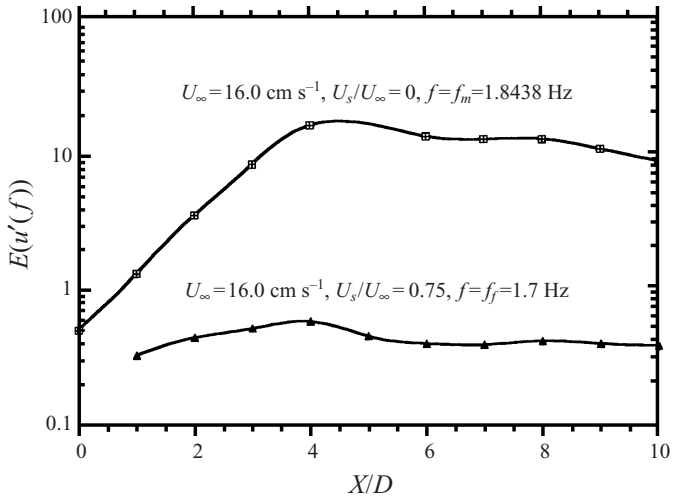

FIGURE 23. Energy content $E(u'(f))$ at the most unstable frequency $f_m = 1.8438$ Hz for $U_s/U_\infty = 0$ and the forcing frequency $f_f = 1.7$ Hz for $U_s/U_\infty = 0.75$.

the phase jitters;

$$E[u'(f)] = \int_{-\infty}^{\infty} [u'(f)]^2 \, \mathrm{d}Y, \tag{8a}$$

where $[u'(f)]^2$ is the narrow-band energy at the frequency f and can be evaluated from the energy spectrum $G[f]$ at the location (X, Y) by the following equation:

$$[u'(f)]^2 = \int_{f-\mathrm{d}f}^{f+\mathrm{d}f} G(f_1) \, \mathrm{d}f_1, \tag{8b}$$

where $\mathrm{d}f$ equals 0.031 Hz.

When suction is not applied, the spatial variation of $E[u'(f)]$ at the unforced fundamental frequency $f_m (= 1.8438$ Hz) is shown in figure 23. Exponential growth of

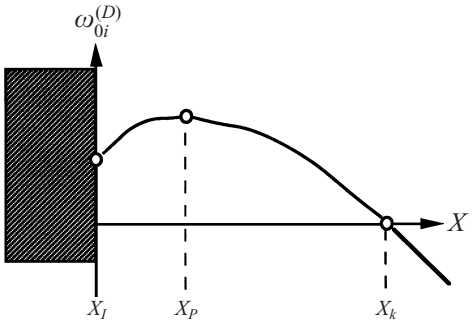

FIGURE 24. Sketch of frequency selection criteria: X_I, initial resonance (Monkewitz & Nguyen); X_P, maximum absolute growth rate (Pierrehumbert); X_k, transition point (Koch).

the disturbances is observed as expected. In the other case, a supercritical suction, $U_s/U_\infty = 0.75$, stabilized the wake. The energy content $E[u'(f)]$ at the forcing frequency $f_f(= 1.7\,\text{Hz})$ in the $U_s/U_\infty = 0.75$ case has a very small amplification rate initially and then remains almost at a constant level. The non-parallel flow caused by suction not only stabilizes the absolute instability but also significantly affects the downstream wake region. The wake flow becomes convectively neutrally stable.

6. The selection of instability frequency

6.1. *Instability frequency and the selection criteria*

From an early work on the examination of the plane wake behind the sharp trailing edge of a flat plate (Masselin & Ho 1985), it was found that the wake vortex passage frequency is the same as the one predicted by the linear spatial stability analysis based upon the velocity profile right at the sharp trailing edge of the splitter plate. The frequencies calculated from downstream velocity profiles do not fit the measured value. After the absolute–convective instability concept was introduced (Huerre & Monkewitz 1985), the physical mechanism governing the above-mentioned phenomenon became clear. The unstable wake is self-excited by the absolute instability in the near-wake region. In the case of a wake developed from a sharp trailing edge, the absolute instability region is very short. Hence, the frequency is likely to be determined by the velocity profile at the trailing edge. In the present experiment, a finite absolutely unstable zone exists. When the suction speed is below the threshold suction, the length of the absolutely unstable region and the amplification rate of the instability vary with the magnitude of suction. The instability frequency must be a function of the suction speed. The question is how the global frequency is selected in a finite absolutely unstable region.

Several researchers have investigated the selection mechanism of the instability frequency in a wake flow (Pierrehumbert 1984; Koch 1985; Monkewitz & Nguyen 1987). They have suggested different criteria for the frequency selection process, based on parallel flow analysis. Pierrehumbert (1984) argued that the flow is dominated by the fastest growing resonance between the downstream and the upstream instability waves. The global response is determined by the maximum growth rate location, X_p, as shown schematically in figure 24. Therefore, the measured frequency is predicted to be equal to the real part of the branch-point frequency at the location X_p, $\omega_{0r}^{(D)}(X_p)$.

Koch (1985), on the other hand, suggested that the transition point in the flow where the branch-point frequency is real acts as an effective 'reflector' for the instability

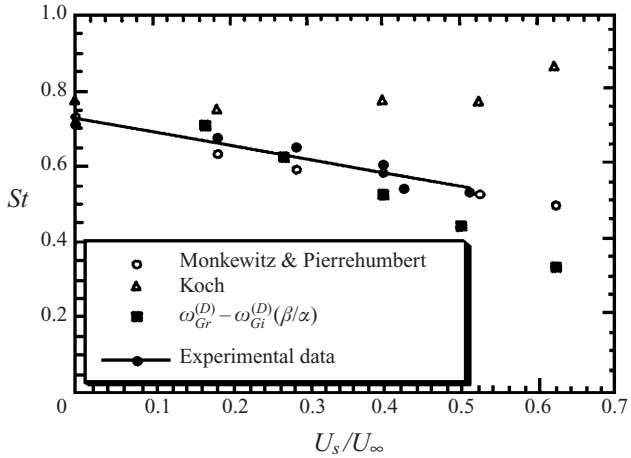

FIGURE 25. Non-dimensional vortex shedding frequency $St\,(=\omega_{or}^{(D)} = 2\pi f D/U_\infty)$ predicted by different frequency selection criteria at various suction speeds ($Re = 1600$).

waves of that particular frequency. Then, the global response is dominated by a local resonance occurring at the transition from the local absolute to the local convective instability. Hence, the global response is determined by the absolute frequency at the transition point X_k where $\omega_{0i}^{(D)}(X_k) = 0$ which is shown in figure 24. In Hanneman & Oertel (1989), the global frequency from their numerical simulations agrees well with the local absolute frequency predicted by Koch's criterion. Oertel (1990) in his review paper showed that the von Kármán vortex street is still dominated by the locally hydrodynamic resonance in the absolutely unstable region at the supercritical Reynolds number even though the Kármán vortex street is in a nonlinear saturated state at that Reynolds number.

Monkewitz & Nguyen (1987) proposed the 'initial resonance criterion'. This criterion suggests that the (non-parallel) wake is dominated by the first local resonance with a non-negative absolute growth rate encountered by the flow. Monkewitz & Nguyen compared this criterion with many experimental results. The predicted frequency agreed with the measured frequency. Therefore, they concluded that the vortex shedding frequency is determined from the most upstream absolutely unstable location, X_I (figure 24).

From our experimental data, the instability frequency selected by the initial resonance criterion (Monkewitz & Nguyen 1987) can be obtained by plotting the frequency $\omega_{0r}^{(D)}$ at the location $X/D = 0$ for different suction speeds (figure 16*b*). The predicted frequencies are shown in figure 25. According to figure 16(*a*), the maximum absolute growth rate occurs at $X/D = 0$. Therefore, the global frequency based on Pierrehumbert's suggestion is the same as that predicted from the initial resonance criterion. From the same sets of data (figure 16), the predicted frequency according to Koch's criterion can be obtained from the real part of the transition-point frequency, $\omega_{0r}^{(D)}(X_k)$, at $\omega_{0i}^{(D)}(X_k) = 0$. The non-dimensional frequencies St, defined as $St = \omega_{0r}^{(D)} = 2\pi f D/U_\infty$, at various suction speeds predicted by the above-mentioned frequency selection criteria are plotted in figure 25. The experimentally determined frequencies are also superimposed on the same figure for easy comparison. It is found that the vortex shedding frequencies agree with Pierrehumbert's criterion as well as with the initial resonance criterion (Monkewitz & Nguyen 1987).

6.2. *Nonlinear analysis of frequency selection*

The instability waves initially amplify exponentially in time at the linear growth rate, ω_{Gi}. At large times, the instability evolves into a nonlinear instability regime (Stuart 1971) and reaches a nonlinear saturation state. In a flow with an extended absolute instability region coupled with a convectively unstable region, it would be interesting to examine the effect of nonlinearity. The dynamics of a weakly nonlinear flow is described by the Stuart–Landau equation:

$$\frac{\mathrm{d}A}{\mathrm{d}t} = [\omega_{Gi} - \mathrm{i}\omega_{Gr}](U_s)A - [l_r + \mathrm{i}l_i]|A|^2 A + O(|A|^5), \tag{9}$$

where A is the amplitude level, ω_{Gi} is the linear temporal global growth rate, ω_{Gr} is the corresponding frequency, and l is the Landau constant. Taylor expanding ω_{Gi}, ω_{Gr} and the saturation frequency ω_{sat} near the threshold suction speed U_{Ts}, the following approximations can be obtained:

$$\omega_{Gi} = \left[\frac{\mathrm{d}\omega_{Gi}}{\mathrm{d}U_s}(U_{Ts})\right][U_s - U_{Ts}] = \alpha[U_{Ts} - U_s], \tag{10a}$$

$$\omega_{Gr} - \omega_{sat} = \left[\frac{\mathrm{d}\omega_{Gr}}{\mathrm{d}U_s}(U_{Ts}) - \frac{\mathrm{d}\omega_{sat}}{\mathrm{d}U_s}(U_{Ts})\right][U_s - U_{Ts}] = \beta[U_s - U_{Ts}], \tag{10b}$$

$$l_r + \mathrm{i}l_i = [l_r + \mathrm{i}l_i](U_{Ts}), \tag{10c}$$

where one can obtain (10*b*) by subtracting two Taylor expansion equations of ω_{Gr} and ω_{sat} and eliminating the high-order terms since ω_{Gr} and ω_{sat} coincide for $U_s = U_{Ts}$. The growth rate ω_{Gi} represents a temporal growth rate. For a positive growth rate, a nonlinear saturation state will be reached.

By setting $\mathrm{d}A/\mathrm{d}t = 0$ in (9), the saturation or limit-cycle amplitude $|A|_{sat}$ for $U_s < U_{Ts}$ is obtained as

$$\omega_{Gi} - \mathrm{i}\omega_{Gr} = [l_r + \mathrm{i}l_i]|A|^2_{sat}, \tag{11a}$$

therefore

$$|A|_{sat} = \left[\frac{\omega_{Gi}}{l_r}\right]^{1/2} = \left[-\frac{\omega_{Gr}}{l_i}\right]^{1/2}. \tag{11b}$$

Introduce the modulus and the phase of A, $A = |A| \exp[-\mathrm{i}\phi]$, into the Stuart–Landau equation. Equation (9) becomes

$$\frac{1}{|A|}\frac{\mathrm{d}|A|}{\mathrm{d}t} = \omega_{Gi} - l_r|A|^2 = \omega_{Gi}\left[1 - \frac{|A|^2}{|A|^2_{sat}}\right], \tag{12a}$$

$$-\frac{\mathrm{d}\phi}{\mathrm{d}t} = -\omega_{Gr} - l_i|A|^2 = -\omega_{Gr} - \omega_{Gi}\left[\frac{l_i}{l_r}\right]\left[\frac{|A|^2}{|A|^2_{sat}}\right]. \tag{12b}$$

When the amplitude $|A|$ reaches the saturation amplitude $|A|_{sat}$, the frequency $\mathrm{d}\phi/\mathrm{d}t$ equals the saturated (measured) frequency, ω_{sat}, i.e. $\mathrm{d}\phi/\mathrm{d}t = \omega_{sat}$. Equation (12*b*) becomes

$$\omega_{Gr} - \omega_{sat} = -\omega_{Gi}\left[\frac{l_i}{l_r}\right]. \tag{13}$$

By using (13), (10*a*) and (10*b*), the ratio l_i/l_r can be obtained as

$$\left[\frac{l_i}{l_r}\right] = -\frac{\omega_{Gr} - \omega_{sat}}{\omega_{Gi}} = -\frac{\beta}{\alpha}. \tag{14}$$

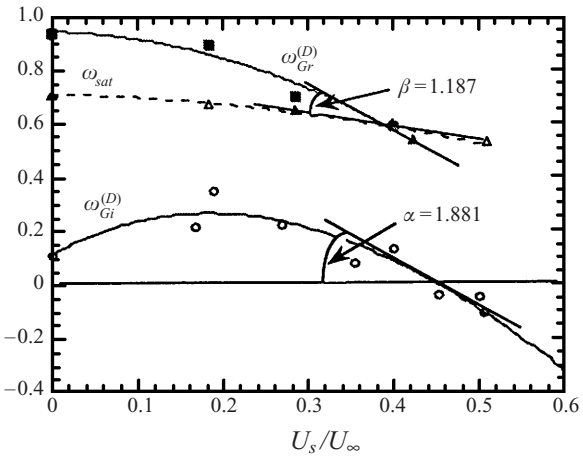

FIGURE 26. Coefficients of Stuart–Landau equation ($Re = 1600$).

Equation (14) shows that the ratio l_i/l_r can be determined by α and β which are defined in (10*a*) and (10*b*) respectively. Figure 25 shows the polynomial curve fitting of non-dimensional real and imaginary parts of the global frequency ($\omega_{Gr}^{(D)}$ and $\omega_{Gi}^{(D)}$ obtained in § 5.3), as well as the saturated vortex shedding frequency ω_{sat} ($= 2\pi f D/U_\infty$ measured by LDA) at different suction speeds. The coefficient of the Stuart–Landau equation is obtained as

$$\left[\frac{l_i}{l_r}\right] \approx -0.6 \tag{15}$$

for the plane wake with base suction.

From the Stuart–Landau model, the nonlinear saturated frequency can be calculated from (13) as

$$\omega_{sat} = \omega_{Gr} + \omega_{Gi}\left[\frac{l_i}{l_r}\right] = \omega_{Gr} - \omega_{Gi}\frac{\beta}{\alpha}. \tag{16}$$

By taking account of frequency shift due to nonlinearity and the fact that the flow with suction is not parallel, (16) has made the connection between the predicted global frequency and the observed shedding frequency in the wake flow with suction speed below the threshold value. The vortex shedding frequency predicted by (16) is plotted in terms of Strouhal number St, which is marked as $\omega_{Gr}^{(D)} - \omega_{Gi}^{(D)}\beta/\alpha$ in figure 25. Both the linear (Pierrehumbert 1984; Monkewitz & Nguyen 1987) and nonlinear stability analysis provide the same trend of decreasing resonance global frequency with increasing suction speeds. However, the quantitative prediction seems worse compared to the criteria of Pierrehumbert and Monkewitz & Nguyen. At this point, why the vortex shedding frequency can be predicted better by simply using the velocity profile at location $X/D = 0$ is still unclear. It is believed that the nonlinear shedding frequency prediction should predict a more 'realistic' frequency since it takes into account the frequency shift due to nonlinearity and the fact that the flow with suction is non-parallel. However, computational errors can be easily introduced into the nonlinear shedding frequency prediction due to its complicated procedures. For example, (13) states that $\omega_{Gr}^{(D)}$ is equal to ω_{sat} when $\omega_{Gi}^{(D)}$ equals zero. In figure 26,

the real part of the global frequency $\omega_{Gr}^{(D)}$ equals to the saturated (or measured) vortex shedding frequency ω_{sat} $(= 2\pi f D/U_\infty)$ at the suction speed $U_s/U_\infty = 0.4$, instead of 0.46 where $\omega_{Gi}^{(D)} = 0$. This discrepancy in determining the coefficients α and β will cause errors in the prediction of the nonlinear shedding frequency. In the present results, the quantitative comparison between the predicted global frequency and the observed shedding frequency in the wake flow strongly suggests that the initial velocity profile plays a very important role in the semi-infinite flow domain. The nearby frequencies related to the initial velocity profile amplified globally in the nonlinear and non-parallel global mode selection process.

6.3. *Sensitivity to external perturbations*

In a self-excited flow such as a wake, it is interesting to find out how the flow responds to the external disturbances, artificial perturbations or background noise. We will examine this problem in the frequency domain. The stabilizing rod placed inside the absolute instability region, $X/D = 0.5$, $Y/D = 0$, serves as a forcing device to generate small-amplitude perturbations in the absolutely unstable region of the wake flow. The amplitude $(= 0.05D)$ used in the present forcing studies is below the required threshold level for lock-in states. The forcing frequency, f_f, of the rod is chosen to be close to the most unstable frequency or the fundamental vortex shedding frequency f_m of the wake; f_m is determined experimentally in the wake without suction as shown in figure 27(*a*). The forcing frequencies, f_f, were varied from 0.9 to 2.4 Hz, covering a range from about $(\frac{1}{2})f_m$ to $1.3f_m$ in the tested range. The energy spectrum measured at a location fairly far downstream from the absolutely unstable region, $X/D = 5.0$, $Y/D = 1.0$, represents the response of the unstable flow to the forcing. The spectral peak is defined as the response frequency, f_r. When $U_s/U_\infty = 0$, the energy spectra at different forcing frequencies are plotted in figure 27. In figure 27(*a*), the peak frequency of the energy spectrum corresponds to the fundamental frequency in the unforced wake flow without suction, f_m. When the control rod vibrator oscillates at 1.5 Hz and at 2.0 Hz, the spectra are shown in figures 27(*b*) and 27(*c*) respectively. The response frequencies in both cases remain unchanged and the peak frequencies are the same as the fundamental frequency in figure 27(*a*), i.e. the flow does not respond to the forcing. Similar results were found in the case of $U_s/U_\infty = 0.25$, where the fundamental frequency is reduced to 1.61 Hz (figure 29). When the suction speed reaches $U_s/U_\infty = 0.56$, unlike the subcritical suction cases in figure 27, the energy spectrum in the unforced wake flow with supercritical suction (figure 28*a*) does not have a clear peak at the most amplified frequency. The self-excited instability disappears and the wake flow becomes stable. The energy spectra at different forcing conditions start to change. Figures 28(*b*) and 28(*c*) show that the spectral peaks are located at the forcing frequency. The wake flow responds to the forcing under the supercritical suction condition. The relationship between the response frequency and the forcing in this suction range is plotted in figure 29.

These results clearly show the difference between a self-excited wake and an externally excited wake. When the wake is self-excited, the frequency is dominated by the intrinsic one determined by the global resonance (for small excitation amplitudes). The external perturbations cannot shift the wake frequency and even have no effect on the energy spectra, which correspond to the narrow-band energy of velocity fluctuation at a specific frequency (figure 27). It is also interesting to see that in the energy spectrum of figure 27(*b*) no peak at all is visible at the forcing frequency of 1.5 Hz. However, in the energy spectrum of figure 28(*b*), the magnitude of the

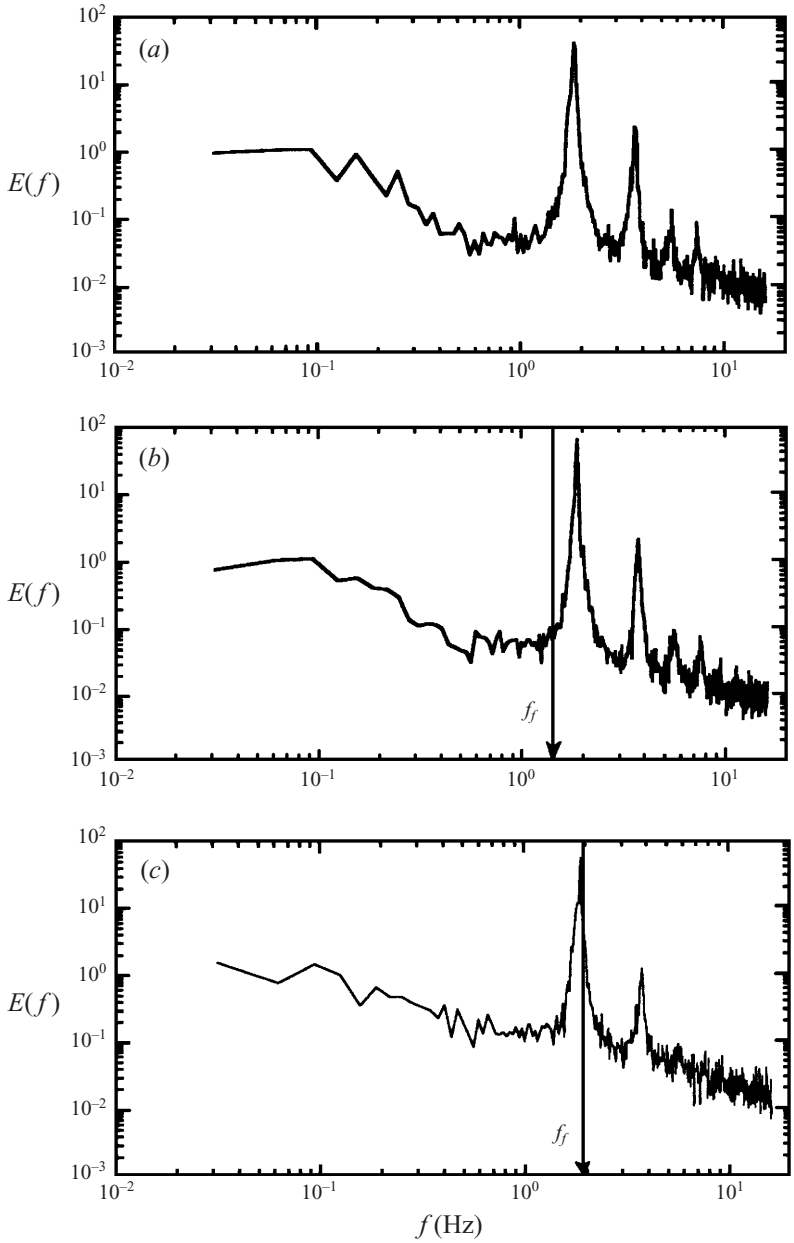

FIGURE 27. Energy spectra at $(X/D, Y/D) = (5.0, 1.0)$ behind the plane wake at $Re = 1600$ with varying forcing frequency: (*a*) $f_f = 0$ Hz; (*b*) $f_f = 1.5$ Hz; (*c*) $f_f = 2.0$ Hz.

peak at 1.5 Hz is significantly above the noise level of the energy spectrum of figure 27(*b*). Since the same amount of energy at the forcing frequency of 1.5 Hz was introduced into figures 27(*b*) and 28(*b*), this suggests that the energy at the forcing frequency 1.5 Hz in figure 27(*b*) is diminished and transferred to the energy at the global resonance frequency. The peak energy in figure 27(*b*) is slightly higher than

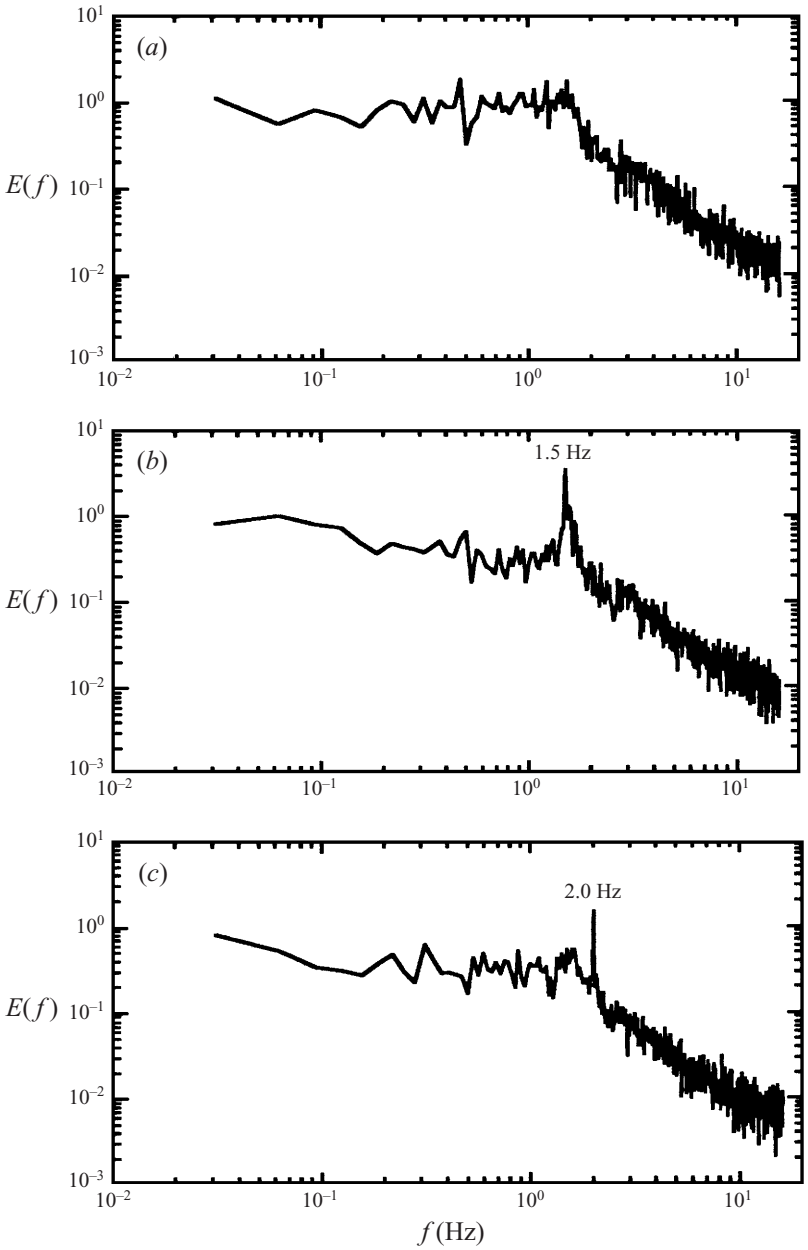

FIGURE 28. Energy spectra $(X/D, Y/D) = (5.0, 1.0)$ behind the plane wake at $Re = 1600$ with suction speed $U_s/U_\infty = 0.56$ and varying forcing frequency: (*a*) $f_f = 0$ Hz; (*b*) $f_f = 1.5$ Hz; (*c*) $f_f = 2.0$ Hz.

that in figure 27(*a*) through the complicated mode interaction or energy transfer in an absolutely unstable flow. When the global instability is turned off, the artificial disturbance becomes detectable and convects in the streamwise direction even though the amplitude will not change in this neutrally stable flow (figure 23). This experiment provides clear evidence of the wake's sensitivity to external noise in a wake.

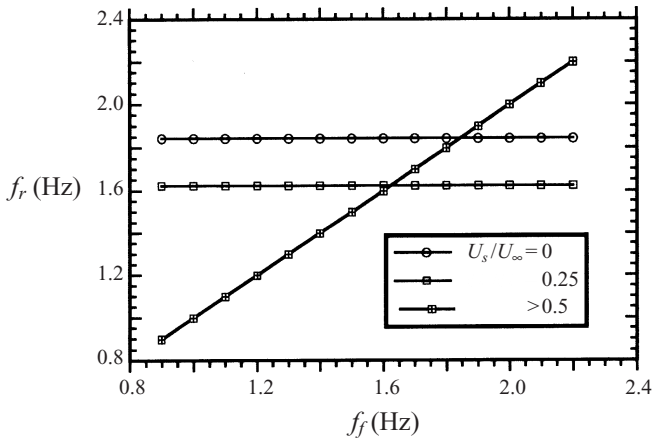

FIGURE 29. The relationship between forcing frequency (f_f) and response frequency (f_r) at different suction speeds ($Re = 1600$, $U_\infty = 16.0\,\mathrm{cm\,s^{-1}}$).

7. Summary

Base suction effectively reduces the size of the absolutely unstable region and forms a non-parallel flow region in the near wake. With the present experiments a threshold suction velocity is found and is approximately equal to half the free-stream velocity. We have made a quantitative link between our plane wake with base suction experiments and weakly non-parallel theory (Monkewitz *et al.* 1993). The threshold velocity can be accurately predicted by global stability analysis with the non-parallel correction. Below the threshold suction, the wake is dominated by self-excitation and is not sensitive to external disturbances. In the case of supercritical suction, the non-parallel flow effect drives the global instability into the stable regime. The entire flow is neutrally stable and a vortex street is not observed. Disturbances convect with the flow at 78% of the free-stream velocity and without much change of the amplitude.

In additional to similarities with the present work, Schumm, Berger & Monkewitz (1994), have applied the theory of Monkewitz *et al.* (1993) using computational data for the wake of a plate (Hanneman & Oertel 1989), and the cylinder wake (Morzynski & Thiele 1993). The discrepancy may account for the difference between the doubly-infinite flow domain feature in the wake of a plate and the semi-infinite flow domain in a plane wake with base suction (Monkewitz *et al.* 1993). In the wake of a plate, according to the analysis in a doubly-infinite flow domain, the saddle point of the complex absolute frequency governs the global behaviour. However, in a plane wake with base suction the global modes are dominated by the absolute frequency at the plate trailing edge. For this reason, we can accurately determine the global modes on the real x-axis in the analysis of our flow experiments.

The authors appreciate Professor Peter Monkewitz's valuable suggestions. This work is mainly supported by a grant from the Office of Naval Research. The early phase of the research was supported by the Air Force Office of Scientific Research.

REFERENCES

BARKLEY, D. & HENDERSON, R. D. 1996 Three-dimensioanl Floquet stability analysis of the wake of a circular cylinder. *J. Fluid Mech.* **322**, 215–241.

BEARMAN, P. W. 1967 The effect of base bleed on the flow behind a two-dimensional model with a blunt trailing edge. *Aero. Q.* **18**, 207–224.

Bender, C. & Orszag, S. 1978 *Advanced Mathematical Methods for Scientists and Engineers.* McGraw-Hill.

Blackwelder, R. F. & Kaplan, R. E. 1976 On the wall structure of the turbulent boundary layer *J. Fluid Mech.* **76**, 89–112.

Chomaz, J. M., Huerre, P. & Redekopp, L. G. 1988 Bifurcation to local and global modes in spatially-developing flows. *Phys. Rev. Lett.* **60**, 25–28.

Chomaz, J. M., Huerre, P. & Redekopp, L. G. 1990 The effect of nonlinearity and forcing on the global modes. In *Proc. Conf on New Trends in Nonlinear Dynamics and Patterning-Forming Phenomena* (ed. P. Coullet & P. Huerre). NATO ASI Series B: vol. 237.

Hammond, D. A. & Redekopp, L. G. 1997 Global dynamics of symmetric and asymmetric wakes. *J. Fluid Mech.* **331**, 231–260.

Hanneman, K. & Oertel Jr. H. 1989 Numerical simulation of the absolutely and convectively unstable wake. *J. Fluid Mech.* **199**, 55–88.

Ho, C. M. & Huang, L. S. 1982 Subharmonics and vortex merging in mixing layers. *J. Fluid Mech.* **119**, 443–473.

Ho, C. M. & Huerre, P. 1984 Perturbed free shear layers. *Ann. Rev. Fluid Mech.* **16**, 365–424.

Huerre, P. & Monkewitz, P. 1985 Absolute and convective instabilities in free shear layers. *J. Fluid Mech.* **159**, 151–168.

Huerre, P. & Monkewitz, P. 1990 Local and global instabilities in spatially developing flows. *Ann. Rev. Fluid Mech.* **22**, 473–537.

Koch, W. 1985 Local instability characteristics and frequency determination of self-excited wake flows. *J. Sound Vib.* **99**, 53–83.

Leu, T. S. 1994 The control of 2-D wakes/mixing layers via suction at the trailing edge of a splitter plate PhD thesis, University of California, Los Angeles.

Leu, T. S. & Ho, C. M. 1992*a* Control of wake-mixing layer flows by suction. *Bull. Am. Phys. Soc.* **37**, 1765.

Leu, T. S. & Ho, C. M. 1992*b* Control of wakes by manipulating mean velocity profiles. *Proc. IUTAM Symp. on Bluff-body wakes, Gottingen, Germany* (ed. H. Eckelmann, J. M. R. Graham, P. Huerre & P. A. Monkewitz), pp. 289–292.

Leu, T. S. & Ho, C. M. 1993 Control of a 2-D wake by suction at the trailing edge of a splitter plate. *Ninth Symp. on Turbulent Shear Flows, Kyoto, Japan Aug. 16–18* (ed. K. Suzuki, F. Durst, N. Kasagi & B. E. Lunder), p. 20-1-1:6.

Masselin, M. & Ho, C. M. 1985 Lock-on and instability in a flat plate wake. *AIAA Paper* 85-0571.

Monkewitz, P. 1988. The absolute and convective nature of instability in two-dimensional wakes at low Reynolds numbers. *Phys. Fluids* **31**, 999–1005.

Monkewitz, P., Huerre, P. & Chomaz, J. 1993 Global linear stability analysis of weakly non-parallel shear flows *J. Fluid Mech.* **251**, 1–20.

Monkewitz, P. & Nguyen, L. N. 1987 Absolute instability in the near-wake of two dimensional bluff bodies. *J. Fluids Struct.* **1**, 165–184.

Morzynski, M. & Thiele, F. 1993 Numerical investigation of wake instabilities. In *Bluff-Body Wakes, Dynamics and Instabilities* (ed. H. Eckelmann, J. M. R. Graham, P. Huerre & P. A. Monkewitz), pp. 135–142. Springer.

Oertel Jr. H. 1990 Wakes behind bluff bodies. *Ann. Rev. Fluid Mech.* **22**, 539–564.

Pierrehumbert, R. T. 1984 Local and global baroclinic instability of zonally varying flow. *J. Atmos. Sci.* **41**, P2141.

Roshko, A. 1955 On the wake and drag of bluff bodies. *J. Aero. Sci.* **22**, 124–132.

Schlichting, H. 1979 *Boundary Layer Theory,* 7th Edn, p. 750. McGraw-Hill.

Schumm M., Berger E. & Monkewitz P. 1994 Self-excited oscillations in the wake of two-dimensional bluff bodies and their control. *J. Fluid Mech.* **271**, 17–53.

Strykowski, P. J. & Niccum, D. L. 1991 The stability of countercurrent mixing layers in circular jets. *J. Fluid Mech.* **227**, 309–343.

Strykowski, P. J. & Sreenivasan, K. R. 1990 On the formation and suppression of the vortex 'shedding' at low Reynolds numbers. *J. Fluid Mech.* **218**, 71–107.

Stuart, J. T. 1971 Nonlinear stability theory. *Ann. Rev. Fluid Mech.* **3**, 347–370.

Wood, C. J. 1964 The effect of base bleed on a periodic wake. *J. Ry. Aero. Soc.* **68**, 643.

Wood, C. J. 1967 Visualization of an incompressible wake with base bleed. *J. Fluid Mech.* **29**, 259–272.

Yu, M. H. & Monkewitz, P. 1990 The effect of nonuniform density on the absolute instability of two-dimensional inertial jets and wakes. *Phys. Fluids* A **2**, 1175–1181.